MODELING AND SIMULATION OF THE EMISSIVITY OF VEGETATION USING PASSIVE REMOTE SENSING METHODS

by

Ali Alperen Şen

B.S., Electrical and Electronics Engineering, Boğaziçi University, 2015

Submitted to the Institute for Graduate Studies in
Science and Engineering in partial fulfillment of
the requirements for the degree of
Master of Science

Graduate Program in Electrical and Electronics Engineering
Boğaziçi University
2019

ACKNOWLEDGEMENTS

Firstly, I would like to express my sincere gratitude to Prof. Selim Şeker, to provide me with all kinds of support in this study. He helped me in determining the subject and also in my long-term studies at very critical points. I completed this work with his high experience, knowledge and important orientations.

Besides, I would like to thank to Asist.Prof. Sema Dumanlı Oktar, who opened the path to work with Prof. Şeker. Besides, I will always remember Prof. Arda D. Yalçınkaya and Assoc. Prof. Fulya Kunter with their good faith, who accepted to take a part in the evaluation committee.

I would like to thank my life friend and my only love Yasemin, who has been with me since the first year of my undergraduate education, whom I married in the master's education, for her contributions in every field of my life. Hope to have a healthy, happy and perfect life together.

I would like to express my deepest gratitude to my parents and my big brother. They have been exemplary to me throughout my life and who have provided me with all kinds of guidance in life. Allah always be with you.

Finally, I would like to thank also to my friends İsmail, Fatih, Murat, Ramazan, Ahmet Emin, Ali İhsan, Emre, Musas and many of other my friends during my undergraduate and graduate studies.

ABSTRACT

MODELING AND SIMULATION OF THE EMISSIVITY OF VEGETATION USING PASSIVE REMOTE SENSING METHODS

Remote sensing is a scientific technique to acquire characteristics of object without physical contact. Gravitational, magnetic, optical and electrostatic forces and resulting actions are sources for remote sensors. Electromagnetic radiation that is emitted or reflected by the object carries specific properties about object. The effect of object on the gathered wave is investigated and some unique properties of the object is obtained with this remote sensing process. To be able to sense complex structures, the structure should be modeled as a familiar geometry. In this thesis, modeling of vegetation and calculated absorption cross section and emissivity simulation was studied. Emissivity is one of frequently used remote sensing parameter for objects. In literature, remote sensing of vegetation includes different methods that are based on measurements with active remote sensing. In this study, vegetation components were considered separately that leaves were modeled as dielectric disks and branches and trunks were modeled as cylinders. Emissivity and absorption cross section equations of geometrically facilitated vegetation was found out using two approximations. Emissivity for leaves was calculated using physical optics approximation on disk. In branches and trunks, infinite length approximation was applied on cylinder. To check the accuracy of equations and MATLAB calculations, absorption cross section calculation results were compared with literature studies on that of vegetation, and good agreement was found. Equations were simulated for frequency, dimensions, angle of incidence, and permittivity. In conclusion, vegetation was geometrically modeled, absorption cross section and emissivity equations were found. Emissivity and absorption cross section were simulated and effects of each parameter was examined.

ÖZET

PASİF UZAKTAN ALGILAMA YÖNTEMLERİNİ KULLANARAK BİTKİ ÖRTÜSÜ EMİSSİVİTESİNİN SİMÜLASYONU VE MODELLENMESİ

Uzaktan algılama, nesnenin fiziksel teması olmadan özelliklerini elde etmek için kullanılan bilimsel bir tekniktir. Yerçekimi, manyetik, optik ve elektrostatik kuvvetler ve bunun sonucunda ortaya çıkan eylemler uzak sensörler için kaynaktır. Nesneden yayılan veya yansıtılan elektromanyetik radyasyon, nesne hakkında belirli özellikler taşır. Nesnenin toplanan dalga üzerindeki etkisi araştırılır ve bu uzaktan algılama işlemi ile nesnenin bazı benzersiz özellikleri elde edilir. Karmaşık yapıları algılayabilmek için nesne bilinen bir geometride modellenmelidir. Bu tez çalışmasında, bitki örtüsünün modellenmesi ve absorbsiyon kesiti ve emisivite hesaplanarak simülasyonu yapılmıştır. Emisivite ve absorbsiyon kesiti, farklı nesneler için sıklıkla kullanılan uzaktan algılama parametresidir. Literatürde, bitki örtüsü uzaktan algılanması çalışmaları, genelde aktif uzaktan algılamalı ölçümlerine dayanan farklı yöntemler içerir. Bu çalışmada, bitki örtüsü bileşenleri ayrı ayrı ele alınmış, yapraklar dielektrik diskler, dallar ve gövde silindir olarak modellenmiştir. İki yaklaşım kullanılarak geometrik olarak kolaylaştırılmış bitki örtüsü yapısına ait pasif algılamada kullanılan emisivite ve absorbsiyon kesit denklemleri bulunmuştur. Yapraklar için emisivite ve absorbsiyon kesiti, disk üzerinde fiziksel optik yaklaşım kullanılarak hesaplanmıştır. Dallar için silindir üzerine sonsuz uzunluk yaklaşımı uygulanmıştır. Denklemlerin ve MATLAB hesaplamalarının doğruluğunu kontrol etmek için, absorbsiyon kesit hesaplama sonuçları, ilgili literatür sonuçları ile karşılaştırılmıştır. Oluşturulan denklemler frekans, boyutlar, geliş açısı ve dielektrik sabiti parametreleri için simüle edilmiştir. Simülasyon sonuçları yorumlanarak her parametrenin etkisi incelenmiştir.

TABLE OF CONTENTS

LIST OF FIGURES

LIST OF TABLES

LIST OF SYMBOLS

a	Disk radius
a_v	Variable radius of disk
B	Bandwidth
c	Speed of light
E_i	Incident electric field
E_{int}^q	Internal electric field
E_q	Internal electric field of infinite length approximation
$e_q(\theta)$	Emissivity of vegetation components
${e_q}^{\pm}$	Wave amplitude
F_n	Transformed electric field inside cylinder
f_v	Variable frequency
G	Amplifier value
$\hat{h}$	Horizontal polarization vector
$\hat{h}_\epsilon^{\pm}$	Horizontal polarization vector inside medium
$\hat{i}$	Incidence vector
J_n	Bessel function of the first kind
k	Plank's constant
k_B	Boltzman constant
L_λ	Spectral radiance
l	Half length of cylinder
n	Number of scatterers per unit volume
$\hat{n}$	Normal vector
$n\Delta z_v$	Variable density of scatterers
$\hat{o}$	Scattering vector
P	Measured radiometer power
P_a	Total absorbed power
$\hat{q}$	Polarization vector
$\hat{q}_\epsilon^{\pm}$	Polarization vector inside medium

r_q	Reflection coefficient
$R_q(\theta)$	Reflection function
$\|S_i\|$	Poynting vector of incident field
T	Kinetic temperature
T_A	Radiometer input temperature
$T_K in$	Kinetic temperature
T_N	Radiometer noise temperature
t_q	Transmission coefficient
$T_q(\theta)$	Reflection coefficient
$T_q^A(\theta)$	Approximate absorbing layer transmission function
V	Volume of absorber object
$\hat{v}$	Vertical polarization vector
$\hat{v}_\epsilon^\pm$	Vertical polarization vector inside medium
w	Angular frequency
$\beta^\pm$	Forward and backward propagation direction
β_z	Normal component of propagation direction
Δz	Height of absorbing layer
δ	Thickness of disk
ε	Emissivity in spectral radiance
ϵ	Radiometer emissivity
ϵ_r	Complex dielectric constant
ϵ_r'	Real component of complex dielectric constant
ϵ_r''	Imaginary component of complex dielectric constant
ϵ_v	Variable complex dielectric constant
η	Intrinsic impedance
θ_i	Angle of incident field
θ_s	Angle of scattered field
θ_v	Variable angle of incidence
λ	Wavelength in spectral radiance
λ_i	Wavelength of incident wave

σ_a	Absorption cross section
$\sigma_a^q(\theta)$	Absorption cross section function
σ_{pq}	Bi-static scattering coefficient
σ_q	Relative permittivity factor
σ_{sim}	Simulated absorption cross section
ϕ_s	Azimuthal angle of scattered wave

LIST OF ACRONYMS/ABBREVIATIONS

CT	Computed Tomography
EM	Electro Magnetic
EMR	Electro Magnetic Radiation
ILC	Infinite Length Cylinder
IR	Infra Red
MRI	Magnetic Resonance Imaging
NASA	National Aeronautics and Space Administration
PO	Physical Optics
UV	Ultra Violet

1. INTRODUCTION

Remote sensing is a scientific method of gathering information about objects without being in physical contact with the object itself. Sensing objects remotely is a process used from the beginning of the earth life. A human utilizes its body organs as sensors to collect and evaluate the information. Scientists developed various remote sensing methods, to be able to detect objects that are not in the range of natural sensory mechanisms. Especially in the last century, technological developments that are taking place rapidly have started to improve remote sensing techniques [6]. Natural forces and actions of the earth provide different methods to sense objects remotely as optical, gravitational, magnetic, acoustic and electromagnetic sensing. In actual meaning, the term "remote sensing" is used for the process of acquiring information with the gathered or sensed reflected or emitted electromagnetic radiation of objects about the Earth's surface [7].

Electromagnetic wave can carry significant and detailed information about places or objects. The wave reflected from the object and sensed with a type of electromagnetic radiation sensor. Electromagnetic wave theory constitutes the base for many research areas, related to the electronic device; however, even for a natural object that does not related with electronics, electromagnetic radiation can be utilized for the information. In remote sensing applications, there are two basic approach that forms the characteristics of the measurement and evaluation process. One is passive remote sensing and the other is active remote sensing. The fundamental difference between these methods is the source of electromagnetic radiation. In passive remote sensing, sun is the source of electromagnetic wave. In active remote sensing, electromagnetic wave provided by the device itself that can also be used for detection of reflected wave [8].

In this thesis, modeling and simulation study of the emissivity of vegetation using passive remote sensing methods will be presented. In Chapter I, remote sensing will be explained in detail as the fundamental step, after a brief introduction on the title of the study. Definitions and related sub-topics will be explained in consideration of

the electromagnetic radiation theory. Researches, developments, and application areas of remote sensing will be mentioned at the end of this chapter. In Chapter II, passive radiometric microwave remote sensing method and approximations will be explained in detail. In this chapter, each component belongs to the vegetation is modeled to obtain computable geometry. In Chapter III, studied model was simulated with unique parameters for absorption cross section and a table is found. The reason for this chapter is to show the accuracy of the model by comparison of absorption cross section result in two studies which are NASA report [9], and a PHD thesis [5] . Chapter IV consists of simulations of modeled vegetation. Then, in Chapter V, simulation results for modeled vegetation will be discussed and at the end of this chapter the study will be concluded.

1.1. Electromagnetic Theory and Remote Sensing

Electromagnetic (EM) energy, characteristics of EM energy and its interactions is a fundamental step to comprehend the remote sensing theory. To understand and to make comment on the remote sensing data, electromagnetic wave theory must be investigated.

The two explained model of EM energy are wave model and photon model. In EM wave model, it is considered that the energy carried in the form of sine waves, and wave propagation is examined in this model. Electric and magnetic fields are perpendicular to each other and the third perpendicular dimension is the propagation direction of the electromagnetic wave. In this direction, both fields propagate through space in the speed of light. These are general explanations about the electromagnetic wave theory, however one of the characteristic parameters of EM wave is significant for the remote sensing modeling and theory that is the wavelength. Wavelength and the frequency are inversely related, because of the constant speed of light [6]. Particle model of the electromagnetic energy is utilized for some applications. Energy of a photon is also related with the frequency of the wave, such that wave of the higher frequency is more energetic. In the physical world, there is a wide range of frequency that begins from the low electric waves and ends with the gamma rays of the atomic nuclei.

The source of EM energy can be any object that has the temperature above the absolute zero, because of the movements of the molecules of the material. Therefore the earth is a source of EM energy, and if it is observed it can be seen that the earth has emission beside the solar radiation reflection. At this point, the term of blackbody has to be defined. Matter called as blackbody can absorb and re-emit all EM energy, and values of the emissivity and absorbance for the blackbodies are both equal to 1. In actual meaning, random motion of the molecules in the matter leads to EM radiation according to the Plank's Law of EM radiation for an ideal source that is the blackbody.

The electromagnetic spectrum is given in Figure1.1 which is the entire range of electromagnetic radiation.

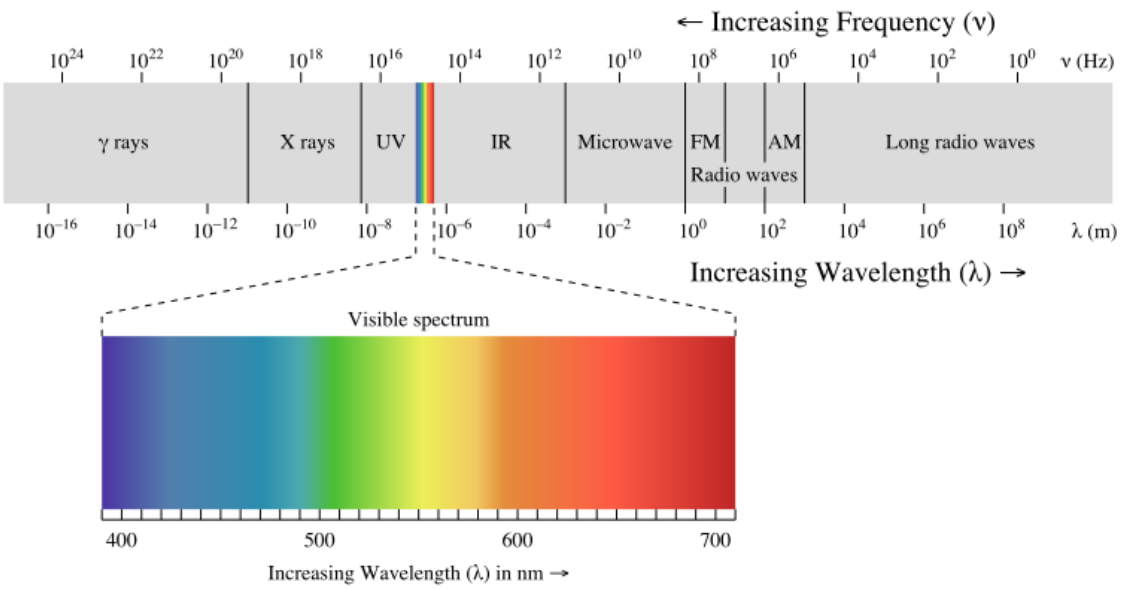

Figure 1.1. Electromagnetic spectrum [1].

Unique energy levels of the electromagnetic spectrum portions are utilized for sensing various materials in the earth. As examples, UV radiation is used to detect some minerals, rocks on the earth surface and as a lower energetic wave type, IR radiation is used frequently in defense systems.

1.1.1. Electromagnetic Interactions

Electromagnetic radiation travels through the atmosphere before it reaches the earth's surface. During this passage, electromagnetic radiation encounters various natural factors as particles and gases, so that some properties of the radiation can be changed in the end. Radiated electromagnetic energy can be immersed, conducted, or reflected through the matter and it also can be scattered and absorbed by the atmosphere. These interactions cause changes in its energy and wave characteristics. In electromagnetic modeling, interactions with the matter and with the atmosphere are investigated to collect information about the object; therefore, EM interactions is explained in two subsections as EM interactions in atmosphere and EM interactions with matter [10].

1.1.1.1. Electromagnetic Interactions In Atmosphere. Electromagnetic radiation carries energy that is inversely proportional with the wavelength. This energy is conserved according to the theory of conservation of energy through the travel in the atmosphere. Hence, EM radiation is either scattered or absorbed in the atmosphere [11]. Scattering the comprehensive definition for reflection and refraction is the unforeseen diffusion of radiation by the particles in the atmosphere. The radiation is also absorbed by the atmosphere and that is actually loss of the radiation energy to atmospheric absorbers.

Electromagnetic radiation is redirected from its original path because of the interactions with the particles and gas molecules in the atmosphere. There are three basic types of scattering. Depending on the wavelength of the radiation, density of the particles and gas molecules, and the travel distance; the amount of scattering changes. The first scattering mechanism is named as Rayleigh scatter.

In common, Rayleigh scatter occurs when radiation interacts with particles that have much smaller diameter than the wavelength of the radiation and atmospheric molecules. The relation between wavelength and the scatter mechanism yield the result that radiation at short wavelengths have stronger tendency to be scattered by

this mechanism. Rayleigh scatter is inversely proportional to the fourth power of radiation wavelength. Additionally, radiation is redirected equally in all directions in this scattering mechanism. In the solar radiation examples of Rayleigh scatter can be seen in daily life as blue sky and red sunset. Travel path of the radiation can change the amount of scattering therefore amount of remaining radiation wavelength [12].

One of the other types of scatter is called as Mie scatter. Mie scatter occurs when radiation encounters with particles that have the diameter between 0.1 to 10 times of the wavelength. Wavelength and scattering intensity have the changing ratio between fourth power of wavelength and the one times wavelength. Water molecules, dust, smoke particles can cause Mie scatter. For longer wavelengths this scattering mechanism is seen in general.

In the interaction with the larger aerosol particles, redirection of radiation is named as nonselective scattering. These particles commonly have 5 to 100 μm diameter size and cause scattering of all visible and IR wavelengths that are reflected. The amount of scattering does not depend on the wavelength, so that the name of this mechanism is nonselective scatter. Water droplets, fog, clouds and ice crystals are main causes. As an example, interaction with clouds means scattering of almost all blue, green or other visible color wavelengths, therefore they can be seen as just in white.

Absorption is the second type of interaction that EM radiation encounters in the atmosphere. Absorption of electromagnetic radiation is a kind of energy conversion mechanism that the energy of the incoming radiation is transferred to absorber molecules. Absorbed energy is converted to heat and gas, so the total energy is conserved in the atmosphere. Ozone, carbon dioxide and water molecules are counted as main reason of absorption in the atmosphere. Ozone absorbs UV and higher frequency radiation and serves us as a conserving layer. For the far infrared region of the spectrum, the critical absorber is carbon dioxide that thermal heating mechanism changes because of the high carbon dioxide density [13, 14]. Some regions exist in the electromagnetic spectrum that at those wavelengths atmosphere let the radiation to transmit

without absorption. Regions of this property is called as atmospheric windows [15]. Transmittance characteristic of the atmosphere is displayed in Figure 1.2.

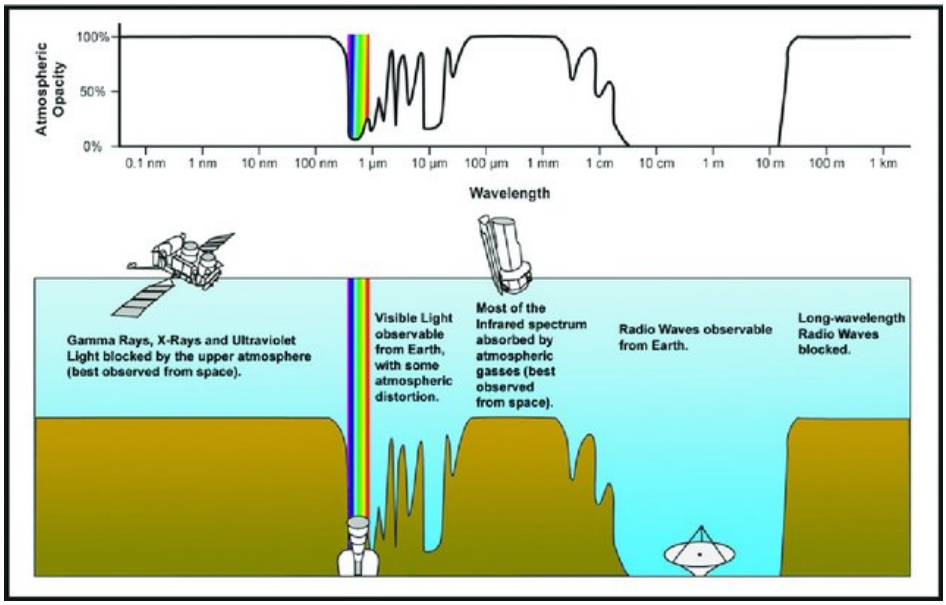

Figure 1.2. Atmospheric transmittance characteristics [2].

Remote sensing applications have to be limited to atmospheric windows, because of the data acquisition availability. A portion in UV, visible light, emitted thermal energy from the earth, microwave energy are counted as atmospheric window regions.

1.1.1.2. Electromagnetic Interactions With Matter. Electromagnetic radiation reaches the earth surface or the surface of the target matter after some loss and scattering. At this time, EMR interacts with the object in three mechanisms. Incoming wave energy can be transmitted, reflected, or absorbed by the object. If the surface of the object is rough that contains small slights, scattering of the wave is also a possible case. Physical and compositional characteristics of the medium effects the action of the radiation. For instance, the shape of the object can cause difference in reflection. In the atomic level, the incoming energy results in an action inside the material atoms, by this way, some electrons can climb to a higher energy level and turn back so that energy is released as photons with this specific energy level.

The wavelength of incident radiation is significant as the material properties. Objects can exhibit different behaviors against the radiation depending on the wavelength. The carried energy may cause or not the expected atomic action. Therefore it can be said that different wavelengths provide detection of different properties of the target object. In Figure 1.3, interaction mechanisms are exhibited.

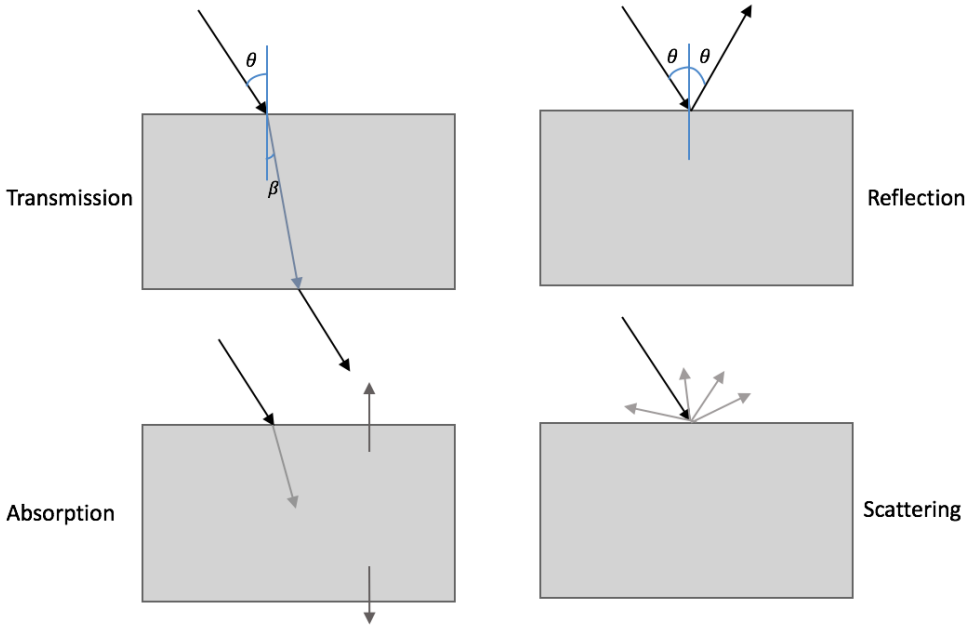

Figure 1.3. Interaction mechanisms between material and incident radiation.

As it can be seen in Figure 1.3, the target object transmits, reflects, scatters or absorbs the radiation and the total energy is constant. Total energy is proportioned between these mechanisms. In remote sensing applications, absorption mechanism holds a significant place. The absorbed energy has to be released or hanged to a form of energy because of the conservation of energy rule. Therefore, in absorption energy is released as thermal radiation in general, and this releasing process represents the emission of the object.

1.1.2. Active Remote Sensing

In active remote sensing, the active sensor provide its own energy source of illumination by emitting the radiation toward the terrain. Backscattered energy of the terrain is collected by the receiver of the active sensor. Airborne and satellite based active sensors emit electromagnetic wave at specific frequency, sense and measure the time, intensity and other characteristics of the backscattered pulses. In this way, transmission and scattering properties of the object that is intended to be sensed can be obtained [3].

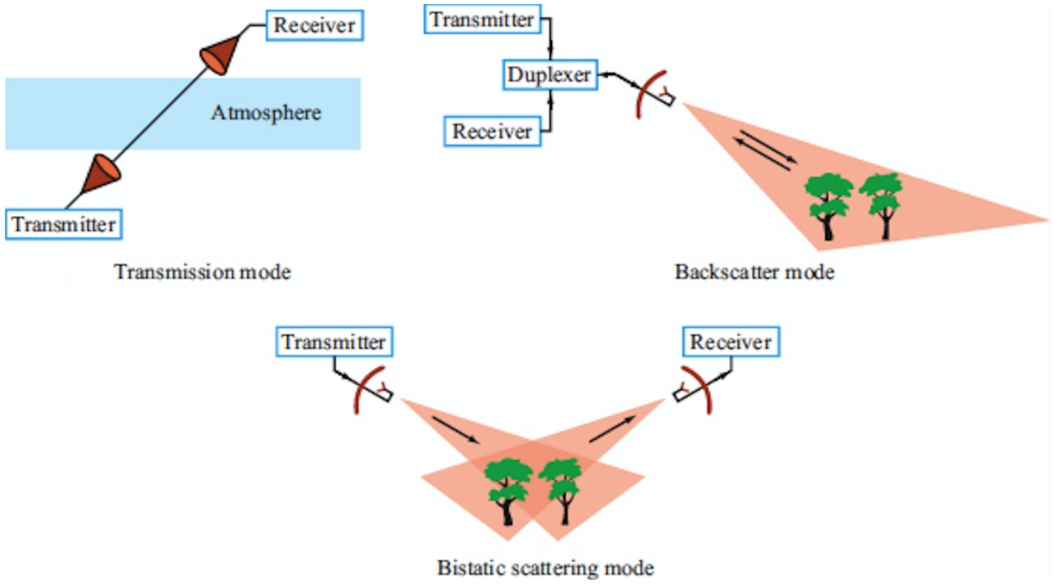

Figure 1.4. Active remote sensing [3].

In the measurement of transmission characteristics of the medium, two antennas are utilized generally as transmitter and receiver on opposite sides of the medium. In scattering measurement, oblique or backscatter modes of radar can be used. Active remote sensing measurement methods are depicted in Figure 1.4. As it can be seen in figure, oblique mode of radar has separated transmitter and receiver that is called as bi-static and as in the backscatter mode transmitter and receiver are at the same location.

The receiver of the radar system measures the power of scattered and collected electromagnetic wave. Radar power equation consists of products of transmitter power, transmitter and receiver gains, loss factors, range between transmitter and target, range between target and receiver, radar wavelength and radar cross section. The last term, radar cross section provides the basis for the information about characteristics of the target [16].

1.1.3. Passive Remote Sensing

Remote sensing process requires a source for electromagnetic radiation that can be provided by an artificial device or by the sun, the natural life source. In passive remote sensing, the source is the solar radiation. In previous subsections it was mentioned that absorption of the radiation by the object produce a form of energy and emits thermal radiation to outside. In addition, some of the materials can reflect the incoming radiation, and forms the radiation for the remote sensor. Therefore, the object depending on its composition and physical properties, forms indirect source of radiation that can be detected by the passive remote sensor [17].

Blackbody radiation was mentioned in previous sections, and that topic summarizes that all object greater than absolute zero emits thermal radiation at different wavelengths. The blackbody radiation curve for the earth displays the maximum emission wavelength range for the earth which is thermal infrared range. Additionally, at the right end of the curve, it can be seen that small amount of energy is transferred with microwave radiation [18]. Blackbody radiation curve for the earth is given in Figure 1.5.

This naturally emitted microwave energy is valuable for remote sensing of the earth, with the advantage of clouds' insignificant microwave range emission that do not interfere with the earth's emission. Passive remote sensing systems does not use only microwave energy. Various studies that utilize wavelengths of electromagnetic spectrum are exist. Film photography is an example for passive remote sensing. Also infrared range of spectrum is used in sensing studies [17]. Radiometry is the technical term

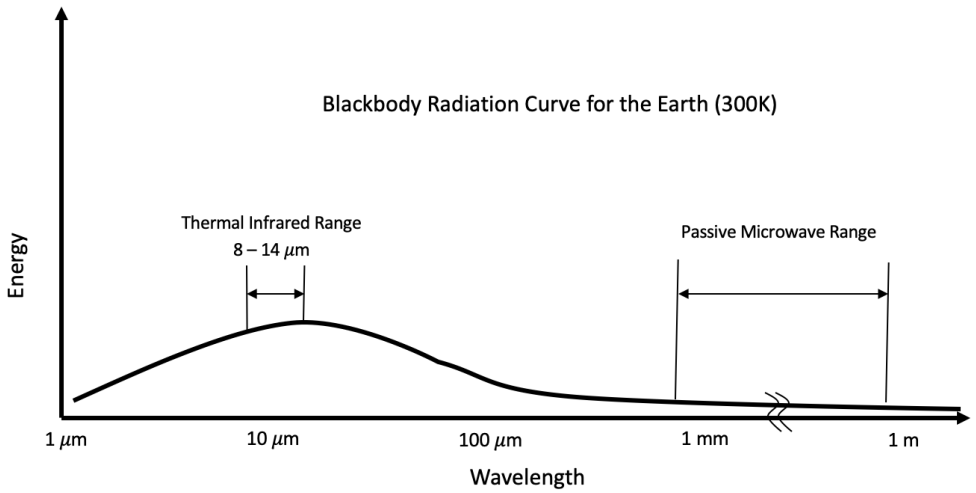

Figure 1.5. Earth's blackbody radiation curve.

for passive sensing of all wavelengths of spectrum that includes all others. Microwave remote sensing has a different role among other investigations, as it is mentioned at first, it enables observations in all weather conditions without any degradation in the information. Unique information about the characteristics of object can be obtained with frequency dependent data of object by utilizing microwave energy [19].

In this study, electromagnetic modeling of vegetation will be examined with microwave passive remote sensing methods. Therefore, basic equations and explanations related to microwave remote sensing will be mentioned.

The microwave portion of the electromagnetic spectrum includes wavelengths from 0.1 mm to 1 m, so that microwave frequency range is between 300 GHz to 0.3 GHz. Radiometers, that are devices for passive remote sensing operate in the range 0.4-35 GHz (0.8-75 cm). If the blackbody radiation curve of the earth is considered, it is seen that the highest radiation is in the range of microwave radiometers. Some other objects as dry ice, liquid air has blackbody radiation curves that follows ideal blackbody radiation curve [6].

Total energy emitted by the blackbody is explained by the Stefan-Boltzmann law, that it is proportional to the T^4. The wavelength of the peak in the spectral radiance curve is described by Wien's displacement law as it is proportional to T^{-1}. Spectral radiance for wavelengths other than the peak wavelength is explained with Rayleigh-Jeans approximation, which is given in Equation 1.1.

$$L_\lambda = \varepsilon \frac{2kcT}{\lambda^4} \tag{1.1}$$

This equation consists of c, speed of light, k, Plank's constant, T, kinetic temperature and ε, that is the emissivity. Microwave radiometers measures emitted spectral radiance that is described in the equation. In addition, approximation equation provides a relationship between emissivity, spectral radiance temperature and wavelength, and that is a linear relationship can be represented by straight line at long wavelengths [6]. In following chapters, equations for emissivity and modeling method will be explained in detail.

1.1.4. Microwave Radiometer Working Principle

Remote sensing process steps will be explained in this section. Remote sensing process begins with the radiation source and ends with the data analysis. Electromagnetic radiation is emitted by the source that can be natural or artificial. The emitted radiation is transferred through the way as atmosphere from source to the object. As it was mentioned in previous sections, the object reflects, transmits or absorbs the radiation. In absorption and reflection case, there will be subsequent emission of radiation in which the object behaves a source. The radiation is transmitted from the object to the sensor. Sensor, depending on its analysis mechanism, converts and transmits the energy of radiation to the ground station. In the ground station, obtained energy is converted to a meaningful digital data and by processing an image belongs to the object is composed [20, 21]. Remote sensing process flow is displayed in Figure 1.6.

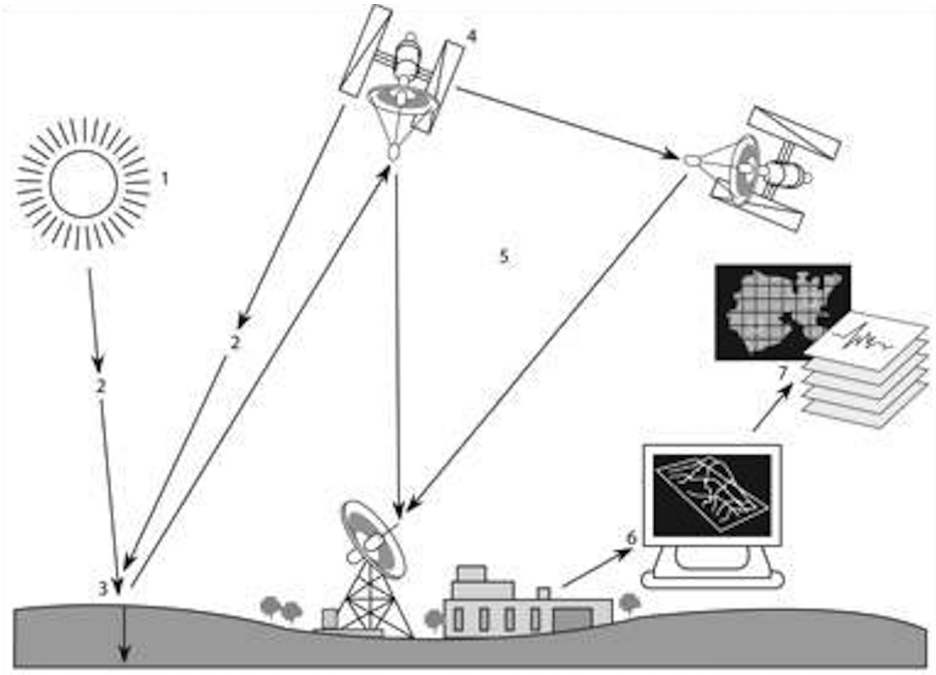

Figure 1.6. Remote sensing process flow [4].

The basic and well known radiometer is Crookes radiometer. It has four vanes in a perfect vacuumed glass tube. When it detects the radiation, they spin. One side of the vanes is black and the other side is white. When strong radiation is detected, it heats up more than absorbed by the dark surfaces of the vanes. Gas molecules hitting these surfaces cause them to rotate. Thus, detected radiation energy is transformed into motion energy. According to rotation speed, the brightness temperature is calculated [22]. Passive microwave radiometer's objective is to measure power that expresses the brightness temperature of the object. There are many advantages working on the passive microwave region. It is independent of weather conditions and atmospheric interactions, wide bandwidth and also objects emit microwave radiation in day and night.

One of the most popular passive microwave radiometer at NASA is AMSR-E. It has twelve-channel, six-frequency (6.925, 10.65, 18.7, 23.8, 36.5, and 89.0 GHz.) and two polarization (vertical and horizontal) [23]. In this thesis study, frequency simulations are done from 4 GHz to 40 GHz.

In literature, emissivity of the object is calculated generally from measured data that comes from the radiometers [6]. The objective of a radiometer is to measure power from its antennas and they are sensitive t measure thermal electromagnetic radiation. In many applications about remote sensing, it is common to express power in terms of brightness temperature. The basic diagram of measurement method of radiometer is shown in Figure 1.7.

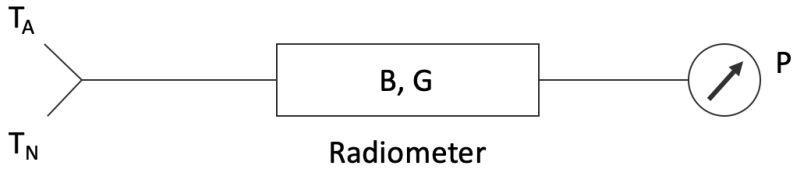

Figure 1.7. Basic diagram of radiometer measurement steps.

A radiometer sense the power emitted from the objects. The basic formula about the power measured from the antennas is given in Equation 1.2.

$$P = k{\cdot}B{\cdot}G{\cdot}(T_A + T_N) \tag{1.2}$$

The equation consist of B, bandwidth , G, amplifier value, k, Boltzman constant that is equal to 1.38×10^{-23} J / K, T_A, input temperature of the radiometer, T_N noise temperature. After calculation of the T_A from Equation 1.2, ϵ, emissivity is calculated from Equation 1.3. In the formula T_{Kin} is kinetic temperature and ϵ is emissivity.

$$T_A = \epsilon{\cdot}T_{Kin} \tag{1.3}$$

In the ideal measurement environment of radiometer, k, B, G and T_N are constant. Although k is always constant, B is generally stable, G and T_N are dependent with the device and environment. To calculate the emissivity from measured power from radiometer, G and T_N should be calibrated and calculated [24]. After calibration, brightness temperature can be calculated from the detected voltages of the radiometer. There are linear relation between measured power and the brightness temperature.

Emissivity value of the object can be calculated from the brightness temperature that is calculated from the measured power. Emissivity is a function of the dielectric constant. Different from the emissivity calculation from the measured power, in this thesis, emissivity of the object is calculated reversely like calculation from the object and its absorption cross section. Estimation of the emissivity before the measurements allows the prediction about the specification of the object and its content. These estimations can be used as the basis for further studies.

1.1.5. Remote Sensing Applications

Remote sensing is a well known research and application area that utilized in various fields. Active and passive remote sensing are both in the interest, because of diversity of being sensed objects in the earth. Application topics were listed and explained to construct an idea about research fields.

- Mineral exploration is one of the fields in which the sensed radiation has different characteristics and carries signatures of each different minerals. In mineral exploration, more energetic radiation is preferred to eliminate the effects coming from compositions of the earth top layer. In the most of studies, the ultraviolet range of the electromagnetic spectrum is utilized [25].
- Soil moisture examination basically related to the amount of water present in the voids between particles in the soil for a certain size. The amount of energy that is radiated from the soil changes depending on the type, amount and water content of the soil. This method provides information about water resources, irrigation, monitoring plant water requirements [26].

- Oceanography is another research field of remote sensing. Electromagnetic emission of oceans gives information about radiant temperature, roughness, color and the depth of the oceans. Chlorophyll content, suspended sediment concentration and coastal zone management are investigated with remote sensing processes [27].
- In the modeling of clouds, after modeling the scattered hydrometeors (rain, snow, ice, etc) in the cloud and calculating the average emissivity, meaningful data about the structure and composition of clouds can be obtained. This technique can be used in space communication and weather forecasting [28].
- Electromagnetic scattering mechanism is very sensitive to permittivity and also water content is a first order determinant of complex permittivity which makes it very useful for remote sensing of water resources. Different frequencies can be used for determining the characteristics of the ground and surface water [29].
- Disasters as earthquake and fire cause sudden changes in thermal radiation that is naturally emitted. This change can be detected by remote sensors that can recognize the action just before or soon after the disaster began. With proper warning systems, precautions and interventions can be carried out [30].
- Investigation of organisms with their surrounding environment is a field of remote sensing. Ecological communities, species assemblages and related conservation precautions is investigated by the help of developing spatial resolution in remote sensing. Change in biodiversity, and loss of special organisms can be observed and future about ecology can be estimated [31].
- In todays diagnostics, remote sensing methods are frequently used. CT (Computed Tomography) and MRI (Magnetic Resonance Imaging) are critical methods in detection of diseases such as tumor radiation, brain structure, thyroid cancer [32].
- The high spatial resolution sensors, laser scanning, data mining and image processing and some other remote sensing technologies, monitoring of urban expansion, changing land usage, urban environment about air pollution and water resources, traffic analysis and other aspects of urban planning can be modeled and planned with remote sensing [33].

- Vegetation covered areas can be counted as special topic in remote sensing applications and studies. Vegetation of an area carries critical signatures, represents different characters that effect the life in a large perspective. Vegetation represents nature and natural resources, so that future plans about the life in the earth requires detailed studies about vegetation. Spectral, spatial, radioactive and temporal characteristics are used to map vegetation with remote sensing. Remote sensing of vegetation is the basic topic of this study, therefore literature review will be indicated in following sections.

1.1.6. Literature Survey on Remote Sensing of Vegetation and Modeling

In literature, there are various studies on remote sensing and vegetation modeling with different perspectives. In the development of technology and research on remote sensing of vegetation, sensing the signature belongs to the vegetation is not only purpose; naturally, vegetation is also a representative layer for soil, moisture and atmospheric gas concentration. In this section, past studies on vegetation modeling related to the remote sensing will be mentioned and in the end the difference of this study will be explained with its contributions.

In soil and moisture research studies, vegetation components are modeled with different methods to collect information about scattering mechanisms and soil characteristics as in [34, 35]. In [36], vegetation is modeled assuming that it is like a layer that consists of only short type of plants. Similarly in [37], emission and absorption of vegetation layer on soil is considered as in the model found by Basharinov and Shutko (1975) and in that the vegetation is a layer which absorbs or emits radiation. Grass and that type of vegetation is also modeled with natural surface interactions in [38].

In a different approach, emissivity of vegetation is modeled in various researches utilizing the dielectric constant as a primary factor. Dielectric constants of unique plant leaves are detected with microwave measurement methods in [39]. Measured dielectric constant is studied with the perturbation model for rough surface to obtain the scattering coefficient. In [40], dielectric constant of sample leaves is measured in simi-

lar way and experimental data is comprised with theoretical data. Dielectric constant calculation or estimation for microwave frequencies can provide a basis for emissivity and remote sensing data analysis steps. Complex dielectric constant is examined for leaves in [41].

Temperature is another frequently used data for investigating emissivity of vegetation. Thermographic camera data is used to evaluate radiation emission and emissivity modeling of vegetation in [42], and resulting emissivities are valid for surface temperature of utilized water bath. Thermal hyper-spectral data, spectrometer data, satellite observations for soil moisture are all different approaches for the evaluation of vegetation emissivity used as in [43,44]. Thermal hyper-spectral data at the vegetation level is investigated in [45], and provided leaf area index is applied in emissivity formula to found the emissivity of selected vegetation component structures.

Brightness temperature is one of the most common used parameters by passive remote sensors. In calculation of brightness temperature, because of the natural restrictions of vegetation and scattering mechanism, resulting formulation based on various assumptions. Brightness temperature is calculated utilizing radiation transfer equations in consideration of energy conservation for a geometrically defined vegetation component structure in [46]. In this model, emissivity is a parameter to calculate the brightness temperature. The emissivity is taken from an other study that models emissivity in terms of scattering coefficients [47].

As a result, surveyed researches and studies were mentioned in this subsection to learn basics about remote sensing of vegetation. Additionally, in the following paragraphs, objectives, differences and contributions of this thesis will be described.

In this thesis, the vegetation component is modeled part by part as discs and cylinders e.g. disk model is used for modeling vegetation leaves and cylinder geometry is utilized for branches and trunks. *Physical Optics* and *Infinite Length* approximations are employed for the derivation of absorption cross section. Absorption cross section derivation is one of the key points to define emissivity. Reflection and transmission

components of the scatterer layer in the emissivity formula are investigated to minimize the effort of mathematical calculation. Resulting emissivity definition is explained with derivation methods. Emissivity of the defined vegetation components are simulated with changing different parameters account in real life.

- Absorption cross section for vegetation components modeled as discs and cylinders was derived, vegetation was not considered as a coverage layer.
- Physical Optics and Infinite Length approximations were used to describe absorption cross section for separate components of vegetation.
- Emissivity formula is investigated to simplify reflection and transmission components.
- Emissivity of a vegetation is simulated for different conditions to provide an applicable useful model results.
- Simulation results of this thesis were compared with literature and agreement was found.
- Obtained simulation result provides data with much cheaper method than experimental process.
- With using parameter simulation MATLAB code written for this thesis study, emissivity and absorption cross section calculations can be made with different variables.

2. EMISSIVITY AND VEGETATION MODELING

Emissivity is the description of radiation emission ability of the subject surface. Emissivity is a dimensionless relative quantity that changes between zero and one. Emissivity value of 1 belongs to the blackbody radiation as it is explained in previous sections [48], and there is no absolute zero emissivity in real, all objects emit radiation to some extent.

In Section 2.1, theory of the emissivity and emissivity formulation will be explained.

2.1. Emissivity Theory

Emissivity of a material can be defined by means of energy conservation relation. The situation is the same for vegetation, as the emissivity is equal to subtraction of reflected and transmitted portions from 1. Emissivity of the vegetation component formula is given in Equation 2.1 [49].

$$e_q(\theta) = 1 - R_q(\theta) - T_q(\theta) \tag{2.1}$$

where;

$$R_q(\theta) = \frac{1}{4\pi} \int_0^{2\pi} \int_0^{\frac{\pi}{2}} \sum_{p=h,v} \frac{\sigma^o_{pq}(\theta, \theta_s, \phi_s - \phi)}{\cos\theta} \sin\theta_s d\theta_s d(\phi_s - \phi) \tag{2.2}$$

$$T_q(\theta) = \frac{1}{4\pi} \int_0^{2\pi} \int_{\frac{\pi}{2}}^{\pi} \sum_{p=h,v} \frac{\sigma'^o_{pq}(\theta, \theta_s, \phi_s - \phi)}{\cos\theta} \sin\theta_s d\theta_s d(\phi_s - \phi) \tag{2.3}$$

In vegetation components' emissivity calculation, the reflected and transmitted portions have to be calculated, however the integral calculations might be troublesome. Here, terms of the integral at first that are $\sigma^{o}_{pq}(\theta, \theta_s, \phi_s - \phi)$ and $\sigma'^{o}_{pq}(\theta, \theta_s, \phi_s - \phi)$ represents bi-static scattering coefficients. Bi-static scattering coefficients are calculated by *Matrix Doubling Method*.

Scattering coefficients for an inhomogeneous irregular layer have been calculated and explained in [50]. If the model that is considered in this study is envisioned, bi-static scattering coefficients have to be analyzed for discs and cylinders. In [51], bi-static scattering coefficients have been investigated for discs and cylinders.

From the average scattering patterns of randomly oriented cylinders and discs have shown that when cylinder dimensions are large with respect to wavelength, bi-static scattering cross sections are peaked in the forward direction.

Dependency on sampling of scattering angle cause the calculation be problematic, therefore an approximation is builded for transmission and reflection behavior of the layer. Based on the average scattering patterns that display a forward behavior it has been assumed that cylinders behave like absorbers. The resulting transmission function equation for the approximate absorbing layer is given in Equation 2.4.

$$T^{A}_{q}(\theta) = \exp -\frac{n\ \Delta z\ \sigma^{q}_{a}(\theta)}{\cos\theta} \tag{2.4}$$

Scatterers amount per unit volume is represented by n. Δz is the layer height. Both of them holds for the density of scatterers in volume. In Equation 2.4, θ represents the angle of incidence and $\sigma^{q}_{a}(\theta)$ represents absorption cross section function.

Because the cylinder layer is considered as an absorbing layer, following approximations in 2.5 and 2.6 are also provided;

$$R_q(\theta) \ll T_q(\theta) \tag{2.5}$$

$$T_q(\theta) \approx T_q^A(\theta) \tag{2.6}$$

Looking back to the first equation in the definition of emissivity of vegetation, the resulting formula holds, Equation 2.7. Absorption cross section term σ_a^q in Equation 2.4 has to be calculated for the conclusion of emissivity equation.

$$e_q(\theta) = 1 - T_q^A(\theta) \tag{2.7}$$

2.2. Absorption Cross Section

Absorption cross section is the most critical term in the definition of emissivity equation as it is mentioned in the previous section. In the definition of absorption cross section first the total power absorbed by a single particle must be considered. The single particle cross section which causes this much absorbed power is called as absorption cross section. A definition for the scattering cross section can be considered in the same way. The total cross section term is the sum of scattering and absorption cross section.

Absorption cross section and electric field relation is the first step for the evaluation of the absorption cross section. An electric field of unit amplitude with $\hat{q}$=($\hat{v}$,$\hat{h}$) is considered to analyze, and it is shown as ${E_{int}}^q$= $\hat{q}e^{-}ik\hat{\imath}.\underline{r}$.

In this representation, k is the wave number. The incidence and scattering directions are shown for impinging field to the lossy dielectric body. The direction of

incidence is symbolized with î and the direction of scattering is symbolized with $\hat{o}$.

Part of the incoming power is absorbed by the object because of the material conductivity or polarization loss. Absorbed power evaluation is the main step to form the absorption cross section equation. Division of total power absorbed by the object to the magnitude of the poynting vector of the incident field gives the absorption cross section [52]. Total power absorbed by the object is formulated in the Equation 2.8.

$$P_a = \frac{w\epsilon_r''}{2} \int_V |{E_{int}}^q(r)|^2 dV \tag{2.8}$$

Absorption cross section σ_a and total power absorbed by the object is related with the following equation;

$$\sigma_a = \frac{P_a}{|S_i|} \tag{2.9}$$

Here $|S_i|$ is the incident Poynting vector for the unit amplitude incident electric field, and it is given in the Equation 2.10

$$|S_i| = \frac{|E_i|^2}{2\eta}\hat{\imath} \tag{2.10}$$

To obtain the absorption cross section, we put the P_a and $|S_i|$ in to Equation 2.9, and resulting equation is;

$$\sigma_a = k\epsilon_r'' \int_V |{E_{int}}^q(r)|^2 dV \tag{2.11}$$

2.3. Vegetation Modeling

Emissivity and back scattering evaluations of vegetation requires a model that relates these characteristics with definable structures in theory. Vegetation components are basically leaves, branches and trunks are considered as absorbing and scattering layers. Leaves of the vegetation is modeled as thin and thick layer of disk shape with complex permittivity. As for branches and trunks, cylinder shape is taken as a basis again with complex permittivity, ϵ_r. The complex permittivity is given in Equation 2.12.

$$\epsilon_r = \epsilon_r' - i\epsilon_r'' \tag{2.12}$$

In complex permittivity equation, first term on the right side is the real part of the complex permittivity. The second term, ϵ_r'' represents the loss factor of the material, therefore with a larger ϵ_r'', the conversion of EM energy to the thermal energy increases.

The definition of absorption cross section provide an insight for the absorption cross section term in the emissivity equation, however the basic problem about this is that the incident electric field is not known exactly. Therefore models for leaves, branches and trunks are used to formulate the electric field with proper approximations and complete solution is found for the absorption cross section.

First of all, the disk and cylinder model of the vegetation components are investigated to understand the scattering and absorbing behavior as lossy structures. Disk and cylinder representations are given in Figure 2.1. a and b are axes of the elliptic disk with thickness of δ and for the cylinder a represents the radius of cylinder. Half length of the cylinder is given as l.

Electric field inside leaves, branches and trunks are calculated with two basic approximations which are explained in following subsections in detail. Leaves are considered as thin and thick disks and the field inside the disk is calculated using

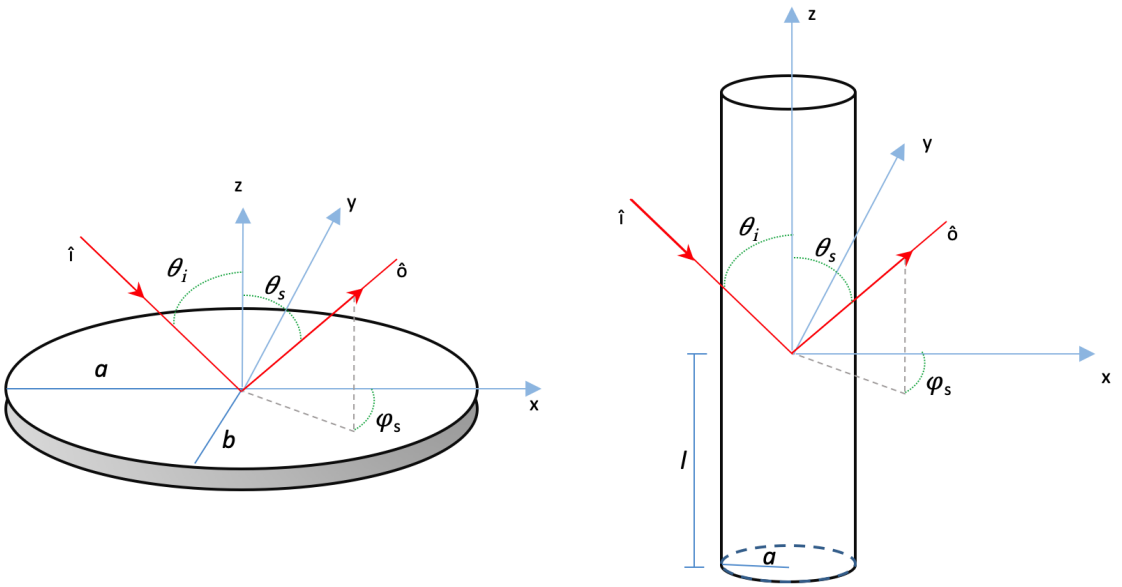

Figure 2.1. Disk and cylinder models.

physical optics approximation. Branches and trunks are considered as cylinders, infinite length approximation is utilized in calculation of field inside the cylinder.

2.3.1. Modeling Of Leaves As Thin and Thick Disks

Leaves of vegetation was investigated in this section and modeled as disks. Physical optics approximation is proper to be employed at this step of the calculation, since the cross section of the disk is large compared with the wavelength. Large cross section with respect to wavelength and thickness provides the advantage of non-effective edges on field.

In the approximation defined as Physical Optics, it is assumed that if the disc axes is large with respect to wavelength of the incident wave, then the disk can be assumed as a slab. Dielectric constant, orientation and the thickness of the slab are the same. The principle behind the approximation is to replace the unknown fielded object to a specific solvable object which is the slab in this case and then to use resulting field description in the object of the study [53, 54].

The incident plane wave is resolved to create two independent wave problems with different polarization. In this way, the field inside the slab is resolved in the same way and each component depends only on the respective incident wave with proper polarization vector. The unit amplitude , polarization $\hat{q}$ incident plane wave is given in Equation 2.13.

$$E_{int}{}^{q}(r,\hat{q}) = \hat{q}e^{(ik_0\hat{\imath}\cdot r)} \tag{2.13}$$

2.3.1.1. Absorption Cross Section of Disk. Figure 2.2 is drawn to display polarization vectors, propagation direction of the incident wave and the dyadic plane wave inside the slab. Horizontal and vertical polarization vectors are $\hat{h}$ and $\hat{v}$ respectively, and inside the slab they are shown as $\hat{h_\epsilon}^{\pm}$ and $\hat{v_\epsilon}^{\pm}$. $\beta^{\pm}$ represents the propagation directions inside. $\hat{n}$ is the unit vector normal to the slab surface.

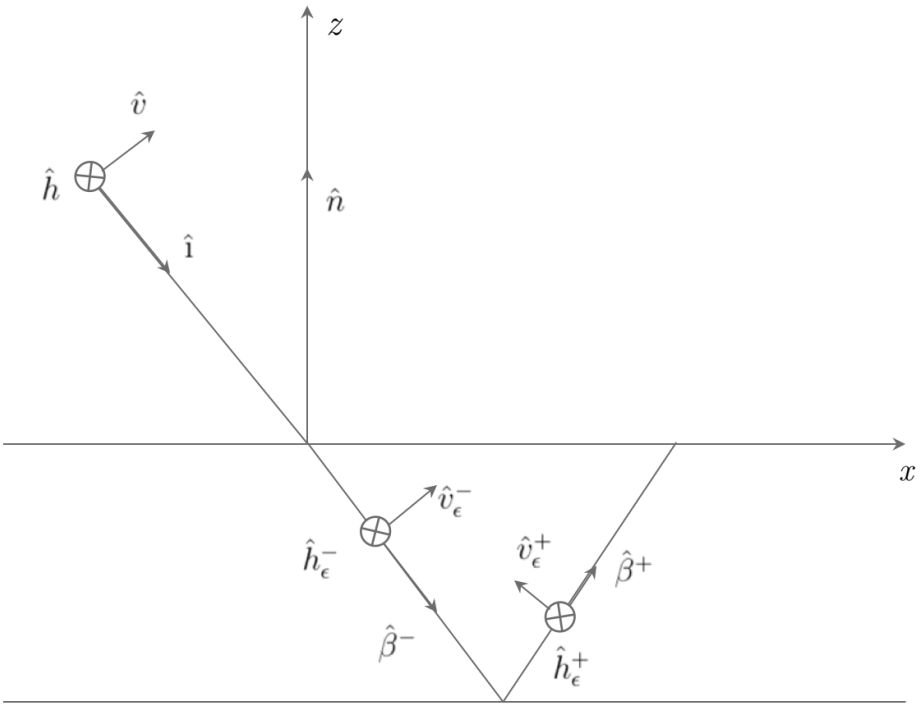

Figure 2.2. Dielectric slab, polarization and propagation vectors.

Solution of Maxwell's equations provides the field definition for slab medium. From that solution, this field is generated by waves with opposite propagation directions with their respective polarization vectors. Therefore the resulting field equation inside the slab is as given in Equation 2.14.

$$E_{int}(r, \hat{q}_\epsilon) = ({e_q}^+ \hat{q}_\epsilon^+ e^{-ik\beta_z z} + {e_q}^- \hat{q}_\epsilon^- e^{ik\beta_z z}) e^{-ik\underline{\beta}_t \cdot \underline{r}_t} \tag{2.14}$$

In this definition, propagation directions are $\underline{\beta}^\pm = \underline{\beta}_t \pm \underline{\beta}_z \hat{n}$. ${e_q}^\pm$ are respective wave amplitudes and $\hat{q}_\epsilon^\pm$ are unit polarization vectors.

In the case of horizontal polarization, $\hat{q}_\epsilon^\pm$ is equal to $\hat{h}_\epsilon^\pm$ that is given in the relation of propagation direction as shown in the Equation 2.15

$$\hat{q}_\epsilon^\pm = \hat{h}_\epsilon^\pm = \frac{\beta^\pm \times \hat{n}}{|\beta^\pm \times \hat{n}|} \tag{2.15}$$

In vertical polarization;

$$\hat{q}_\epsilon^\pm = \hat{v}_\epsilon^\pm = \hat{h}_\epsilon^\pm \times \beta \tag{2.16}$$

Remaining undefined component in Equation 2.14 is the amplitude for forward and backward directions inside the slab. ${e_q}^+$ and ${e_q}^-$ are defined in following equations.

$${e_q}^+ = -\frac{t_q r_q e^{i\psi}}{1 - r_q^2 e^{i\psi}} e^{i\alpha(\hat{\imath} + \underline{\beta}^-) \cdot \hat{n}} \tag{2.17}$$

$${e_q}^- = \frac{t_q}{1 - r_q^2 e^{i\psi}} e^{i\alpha(\hat{\imath} + \underline{\beta}^+) \cdot \hat{n}} \tag{2.18}$$

$\alpha = \frac{1}{2} kl$ and $\psi = 4\alpha\beta_z$. Transmission and reflection coefficients for the slab are t_q and r_q respectively. These coefficients are scalar characteristic parameters of the dielectric material of the slab. The dependency on the material or the material specification

is included in the equation with these parameters. Equation 2.19 and Equation 2.20 describes transmission and reflection coefficients for the slab.

$$t_q = \frac{2\sqrt{\sigma_q}(\hat{\imath} \cdot \hat{n})}{(\hat{\imath} \cdot \hat{n}) - \sigma_q(\underline{\beta}^+ \cdot \hat{n})} \tag{2.19}$$

$$r_q = \frac{(\hat{\imath} \cdot \hat{n}) + \sigma_q(\underline{\beta}^+ \cdot \hat{n})}{(\hat{\imath} \cdot \hat{n}) - \sigma_q(\underline{\beta}^+ \cdot \hat{n})} \tag{2.20}$$

In these expressions, σ_q is the representative factor for relative permittivity and relative permeability of the dielectric, the slab. In this case, because the slab or the original material is non-magnetic, relative permeability is not effective, meanly it is 1. Therefore, according to the polarization, σ_q is given as in the Equation 2.21 [55].

$$\sigma_q = \begin{cases} 1 & \text{if} \quad \hat{q} = \hat{h} \\ \frac{1}{\epsilon_r} & \text{if} \quad \hat{q} = \hat{v} \end{cases} \tag{2.21}$$

Expressions of all mentioned above is to obtain the electric field expression in the slab and by this way in the thin and thick disks model for the absorption cross section of leaves of vegetation. At the beginning of the physical optics approximation, the absorption cross section expression is known as in Equation 2.22, so $|E_{int}|^2$ must be defined.

$$\sigma_a = k\epsilon_r'' \int_V |{E_{int}}^q(r)|^2 dV \tag{2.22}$$

$|E_{int}^q|^2$ is obtained from the dot product of ${E_{int}}^q$ and its complex conjugate;

$$|E_{int}^q|^2 = ({e_q}^+ \hat{q}_\epsilon^+ e^{-ik\beta_z z} + {e_q}^- \hat{q}_\epsilon^- e^{ik\beta_z z}) \cdot ({e_q}^{+*} \hat{q}_\epsilon^{+*} e^{ik\beta_z^* z} + {e_q}^{-*} \hat{q}_\epsilon^{-*} e^{-ik\beta_z^* z}) \tag{2.23}$$

Since $\hat{q}_\epsilon^{\pm}$ is the unit polarization vector inside the slab, $\hat{q}_\epsilon^{\pm} \cdot \hat{q}_\epsilon^{\pm *} = 1$.

$$|E_{int}^q|^2 = |{e_q}^+|^2 e^{-ik(\beta_z - {\beta_z}^*)z} + |{e_q}^-|^2 e^{ik(\beta_z - {\beta_z}^*)z} + {e_q}^+ {e_q}^{-*} \hat{q}_\epsilon^+ \cdot \hat{q}_\epsilon^{-*} e^{-ik(\beta_z + {\beta_z}^*)z}$$

$$+ {e_q}^- {e_q}^{+*} \hat{q}_\epsilon^- \cdot \hat{q}_\epsilon^{+*} e^{ik(\beta_z + {\beta_z}^*)z} \tag{2.24}$$

$$|E_{int}^q|^2 = |{e_q}^+|^2 e^{2kIm(\beta_z)z} + |{e_q}^-|^2 e^{-2kIm(\beta_z)z} + {e_q}^+ {e_q}^{-*} \hat{q}_\epsilon^+ \cdot \hat{q}_\epsilon^{-*} e^{-2ikRe(\beta_z)z}$$

$$+ {e_q}^- {e_q}^{+*} \hat{q}_\epsilon^- \cdot \hat{q}_\epsilon^{+*} e^{2ikRe(\beta_z)z} \tag{2.25}$$

From Equation 2.25, $|{E_{int}}^q|^2$ is known. The volume integral in Equation 2.11 can be solved by using disk dimensions, because the change in the inner field depends only on the variable z.

$$\int_V |E_{int}^q|^2 dV = \pi ab \int_{-\frac{\delta}{2}}^{\frac{\delta}{2}} |{E_{int}}^q(r)|^2 dz \tag{2.26}$$

Utilizing the resulting $|E_{int}|^2$ in Equation 2.26, following expression is obtained;

$$\pi ab \int_{-\frac{\delta}{2}}^{\frac{\delta}{2}} |E_{int}(r)|^2 dz = \pi ab \Bigg[|{e_q}^+|^2 \frac{\sinh\left(k\delta Im(\beta_z)\right)}{kIm(\beta_z)} |{e_q}^-|^2 \frac{\sinh\left(k\delta Im(\beta_z)\right)}{kIm(\beta_z)}$$

$$+ {e_q}^+ {e_q}^{-*} \hat{q}_\epsilon^+ \cdot \hat{q}_\epsilon^{-*} \frac{\sin\left(k\delta Re(\beta_z)\right)}{kRe(\beta_z)}$$

$$+ {e_q}^- {e_q}^{+*} \hat{q}_\epsilon^- \cdot \hat{q}_\epsilon^{+*} \frac{\sin\left(k\delta Re(\beta_z)\right)}{kRe(\beta_z)} \Bigg] \tag{2.27}$$

Lastly, collecting the integral and terms on the right side; absorption cross section of the disk is founded as given in Equation 2.28, here Re and Im are real and imaginary part operators of complex components.

$$\sigma_a^q = k\epsilon_r'' ab\delta \left[(|e_q^+|^2 + |e_q^-|^2) \frac{\sinh(k\delta Im(\beta_z))}{k\delta Im(\beta_z)} + 2Re(e_q^+ \hat{q}_\epsilon^+ \cdot e_q^{-*} \hat{q}_\epsilon^{-*}) \frac{\sin(k\delta Re(\beta_z))}{k\delta Re(\beta_z)} \right] \quad (2.28)$$

2.3.2. Modeling Of Branches and Trunks As Cylinders

Branches and trunks of the vegetation has an expression for absorption cross section similar to leaves mentioned in previous section. Similarly, for the calculation of absorption cross section of a modeled branch which is a cylinder, square of electric field inside the cylinder medium has to be evaluated.

Electric field expression is obtained utilizing a proper approximation which is chosen according to the geometrical relation. Cylinder shown in Figure 2.1 is $2l$ long with a radius and complex permittivity constant $\epsilon = \epsilon_r' + \epsilon_r''$. In the case of the relation that $kl \gg 1$, Infinite Length Approximation is appropriate to derive the expression for electric field inside the cylinder [56]. In this approximation, electric field inside a finite length cylinder is assumed that it is similar to the infinite length cylinder with same orientation and permittivity [57].

$$\sigma_a^q = k\epsilon_r'' \int_V |{E_{int}}^q(r)|^2 dV \quad (2.29)$$

For the sake of simplicity, E^q will be used instead of E_{int}^q in the following equations representing the q polarized incident field. Axes of the cylinder is aligned with the z axes of the cartesian coordinate.

Considering the field inside the infinite length cylinder, the field inside the cylinder under evaluation is formulated, and it is the sum of electric field components of x, y

and z axes [54].

$$E^q = E^q_x\hat{x} + E^q_y\hat{y} + E^q_z\hat{z} \tag{2.30}$$

x, y and z axes components are described by following equations. These equations are created by matching the tangential components of field's boundary conditions at the cylinder surface. In that, θ and ϕ represents polar angles of incident electric field.

$$E^q_x = \sum_{n=-\infty}^{\infty} F_n\left[c^q_n J_{n+1}(\lambda_i\rho)e^{i\phi} + d^q_n J_{n-1}(\lambda_i\rho)e^{-i\phi}\right] \tag{2.31}$$

$$E^q_y = -i\sum_{n=-\infty}^{\infty} F_n\left[c^q_n J_{n+1}(\lambda_i\rho)e^{i\phi} - d^q_n J_{n-1}(\lambda_i\rho)e^{-i\phi}\right] \tag{2.32}$$

$$E^q_z = \sum_{n=-\infty}^{\infty} F_n\left[e^q_n J_n(\lambda_i\rho)\right] \tag{2.33}$$

Infinite sum of cylindrical wave functions, provides transformed electric field expressions inside the cylinder.

$$F_n = E_o i^{-n} e^{in\phi + ikz\cos\theta} \tag{2.34}$$

In these equations, there are some parameters, given in following equations. These parameters are related with the unknown coefficients, that are extracted from boundary

conditions for three axes.

$$c_n^q = \frac{k}{2\lambda_i}(\eta h_n^q - i e_n^q \cos\theta) \tag{2.35}$$

$$d_n^q = \frac{k}{2\lambda_i}(\eta h_n^q + i e_n^q \cos\theta) \tag{2.36}$$

$$e_n^v = \frac{i\sin\theta}{R_n J_n(u)}\left(\frac{H_n^{'(2)}(v)}{vH_n^{(2)}(v)} - \mu_r \frac{J_n{}'(u)}{uJ_n(u)}\right) \tag{2.37}$$

$$h_n^v = \frac{\sin\theta}{\eta R_n J_n(u)}\left(\frac{1}{v^2} - \frac{1}{u^2}\right) n\cos\theta \tag{2.38}$$

$$e_n^h = \frac{-\sin\theta}{R_n J_n(u)}\left(\frac{1}{v^2} - \frac{1}{u^2}\right) n\cos\theta \tag{2.39}$$

$$h_n^h = \frac{i\sin\theta}{\eta R_n J_n(u)}\left(\frac{H_n^{'(2)}(v)}{vH_n^{(2)}(v)} - \epsilon_r \frac{J_n{}'(u)}{uJ_n(u)}\right) \tag{2.40}$$

$$R_n = \frac{\pi v^2 H_n^{(2)}}{2}\left[\left(\frac{H_n^{'(2)}(v)}{vH_n^{(2)}(v)} - \mu_r \frac{J_n{}'(u)}{uJ_n(u)}\right)\left(\frac{H_n^{'(2)}(v)}{vH_n^{(2)}(v)} - \epsilon_r \frac{J_n{}'(u)}{uJ_n(u)}\right) - \left(\frac{1}{v^2} - \frac{1}{u^2}\right) n^2 \cos\theta^2\right] \tag{2.41}$$

In the end, an expression for the internal electric field of cylinder with infinite length is derived, however the necessary expression is the modulus of squared inner field. Therefore in the following, sum of modulus of squared inner fields for three axes is derived. In absorption cross section equation this derivation will be used.

$$|E^q|^2 = |E_x^q|^2 + |E_y^q|^2 + |E_z^q|^2 \tag{2.42}$$

Each of them are extracted separately,

$$|E_x^q|^2 = \left|\sum_{n=-\infty}^{\infty} F_n c_n^q J_{n+1}(\lambda_i \rho)\right|^2 + \left|\sum_{n=-\infty}^{\infty} F_n d_n^q J_{n-1}(\lambda_i \rho)\right|^2$$

$$+ e^{-2i\phi} \sum_{n=-\infty}^{\infty} F_n d_n^q J_{n-1}(\lambda_i \rho) \sum_{m=-\infty}^{\infty} F_m^* c_m^{q*} J_{m+1}(\lambda_i \rho)$$

$$+ e^{2i\phi} \sum_{n=-\infty}^{\infty} F_n c_n^q J_{n+1}(\lambda_i \rho) \sum_{m=-\infty}^{\infty} F_m^* d_m^{q*} J_{m-1}(\lambda_i \rho) \tag{2.43}$$

$$|E_y^q|^2 = \left| \sum_{n=-\infty}^{\infty} F_n c_n^q J_{n+1}(\lambda_i \rho) \right|^2 + \left| \sum_{n=-\infty}^{\infty} F_n d_n^q J_{n-1}(\lambda_i \rho) \right|^2$$

$$-e^{-2i\phi} \sum_{n=-\infty}^{\infty} F_n d_n^q J_{n-1}(\lambda_i \rho) \sum_{m=-\infty}^{\infty} F_m^* c_m^{q*} J_{m+1}(\lambda_i \rho)$$

$$-e^{2i\phi} \sum_{n=-\infty}^{\infty} F_n c_n^q J_{n+1}(\lambda_i \rho) \sum_{m=-\infty}^{\infty} F_m^* d_m^{q*} J_{m-1}(\lambda_i \rho) \tag{2.44}$$

$$|E_z^q|^2 = \left| \sum_{n=-\infty}^{\infty} F_n e_n^q J_n(\lambda_i \rho) \right|^2 \tag{2.45}$$

The squared modulus of inner field is derived and given in Equation 2.46. In absorption cross section equation, volume integral is seen as the next step.

$$|E^q|^2 = \left| \sum_{n=-\infty}^{\infty} F_n c_n^q J_{n+1}(\lambda_i \rho) \right|^2 + \left| \sum_{n=-\infty}^{\infty} F_n d_n^q J_{n-1}(\lambda_i \rho) \right|^2$$

$$+ \left| \sum_{n=-\infty}^{\infty} F_n e_n^q J_n(\lambda_i \rho) \right|^2 \tag{2.46}$$

Volume intergal;

$$\int_V |E^q|^2 dV = \int_{-l}^{l} \int_0^a \int_0^{2\pi} |E^q|^2 \rho \; d\rho \; d\phi \; dz \tag{2.47}$$

Separate solution for $d\rho \; d\phi \; dz$ is used and for the z coordinate we have;

$$\int_{-l}^{l} e^{ikz\cos\theta} e^{-ikz\cos\theta} \; dz = 2l \tag{2.48}$$

Secondly, $d\phi$, that is azimuthal coordinate is calculated as;

$$\int_0^{2\pi} \left| \sum_{n=-\infty}^{\infty} F_n e_n^q J_n(\lambda_i \rho) \right|^2 \; d\phi$$

$$= \int_0^{2\pi} \sum_{n=-\infty}^{\infty} F_n e_n^q J_n(\lambda_i \rho) \sum_{m=-\infty}^{\infty} F_m^* e_m^{q*} J_m^*(\lambda_i \rho) \; d\phi$$

$$= \int_0^{2\pi} \left[\sum_{n=-\infty}^{\infty} i^{-n} E_o e^{in\phi} e_n^q J_n(\lambda_i \rho) \sum_{m=-\infty}^{\infty} -i^{-m} E_o^* e^{-im\phi} e_m^{q*} J_m^*(\lambda_i \rho) \right] d\phi$$

$$= 2\pi |E_o|^2 \sum_{n=-\infty}^{\infty} e_n^q J_n(\lambda_i \rho) e_n^{q*} J_n^*(\lambda_i \rho)$$

$$= 2\pi \sum_{n=-\infty}^{\infty} \left|e_n^q J_n(\lambda_i \rho)\right|^2 \tag{2.49}$$

with $|E_o|^2 = 1$.

$$\int_0^{2\pi} \left| \sum_{n=-\infty}^{\infty} F_n c_n^q J_{n+1}(\lambda_i \rho) \right|^2 d\phi = 2\pi \sum_{n=-\infty}^{\infty} \left|c_n^q J_{n+1}(\lambda_i \rho)\right|^2 \tag{2.50}$$

$$\int_0^{2\pi} \left| \sum_{n=-\infty}^{\infty} F_n d_n^q J_{n-1}(\lambda_i \rho) \right|^2 d\phi = 2\pi \sum_{n=-\infty}^{\infty} \left|d_n^q J_{n-1}(\lambda_i \rho)\right|^2 \tag{2.51}$$

For the radial coordinate, including results from previous equations,

$$\int_0^a \left[\sum_{n=-\infty}^{\infty} \left|e_n^q J_n(\lambda_i \rho)\right|^2 + 2 \sum_{n=-\infty}^{\infty} \left|c_n^q J_{n+1}\right|^2 + 2 \sum_{n=-\infty}^{\infty} \left|d_n^q J_{n-1}\right|^2 \right] \rho d\rho$$

$$= \sum_{n=-\infty}^{\infty} |e_n^q|^2 Y_n + 2|c_n^q|^2 Y_{n+1} + 2|d_n^q|^2 Y_{n-1} \tag{2.52}$$

Equation 2.52, represents the squared modulus of inner field.

In the final expression the Y_n term causes from integrals of Bessel functions of the first kind, which come from the beginning of the inner field expression for cylindrical wave transformation.

$$Y_n = \int_0 J_n(\lambda_i \rho) J_n^*(\lambda_i \rho) \rho d\rho = \int_0^a J_n(\lambda_i \rho) J_n(\lambda_i^* \rho) \rho d\rho$$

$$= \frac{a}{\lambda_i^2 - \lambda_i^{*2}} [\lambda_i J_n(\lambda_i^* a) J_{n+1}(\lambda_i a) - \lambda_i^* J_n(\lambda_i a) J_{n+1}(\lambda_i^* a) \tag{2.53}$$

Absorption cross section equation is the latest and the most critical step in the derivation of emissivity equation for a modeled branch. Using the following equation and emissivity equations in section 2.1, Emissivity value is obtained for a branch. Absorption cross section is also an important parameter indicating properties of subject material.

$$\sigma_a^q = 4\pi k \epsilon_r'' l \left(\sum_{n=-\infty}^{\infty} |e_n^q|^2 Y_n + 2|c_n^q|^2 Y_{n+1} + 2|d_n^q|^2 Y_{n-1} \right) \tag{2.54}$$

3. MODEL ACCURACY AND LITERATURE COMPARISON

The aim of this chapter is to present the accuracy of created model by comparisons. In literature, disk and cylinder models were used for absorption and scattering cross section calculations with various materials. In these studies, absorption cross section was also calculated for vegetation parameters using similar approximations, however the simulation tool and method is different. Therefore, comparison of results with literature provides accuracy of model.

3.1. Thesis Study Comparison

Firstly, absorption cross section was simulated for frequency parameter using same vegetation characteristics and same angle of incidence in [5]. Frequency range in these graphs, includes low and high frequencies. Frequency restriction for the approximation was mentioned in theory part. That is the wavelength must be smaller than the disk radius to assume non-effective edges for calculation. At low frequencies, wavelength is larger than disk cross section, the use of physical optics approximation is not effective.

In simulation, angle of incidence is taken as 0^o and disk radii is 7.0 cm. Thickness of the disk is 0.3 mm. Frequency range was selected as low frequency and high frequency values included, from 1 GHz to 40 GHz.

As we observe two curves in Figure 3.1, it is seen that both graphs increases with decreasing slope. This is an expected situation. At low frequencies, meanly from 1 GHz to 5 GHz, shape of graphs are similar, however absorption cross section values are different. Low frequency region displays the reason of approximation restriction. Error percentage is larger than increased frequency regions.

Frequencies around 5 GHz absorption cross section values become consistent with. $10^{-}3$ is reached at 10 GHz frequency and slope is decreased. In comparison of values at 5 GHz, 10GHz, 20 GHz and 40 GHz, absorption cross section values are consistent.

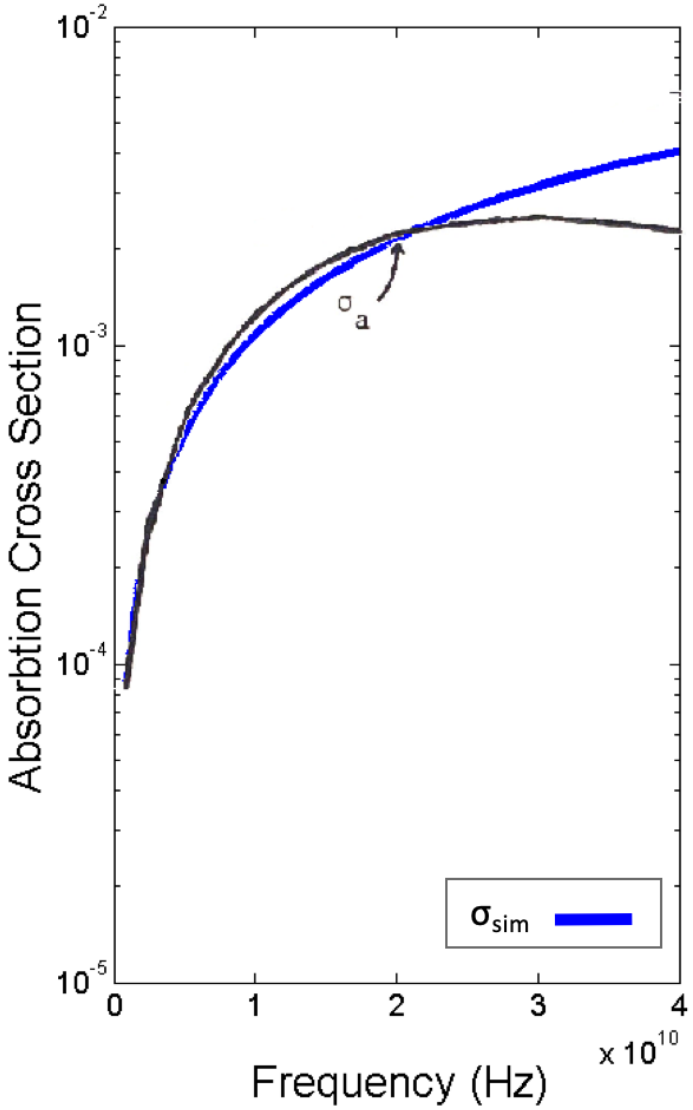

Figure 3.1. Absorption cross section σ_a in [5] and σ_{sim} in simulation.

3.2. NASA Report Comparison

In second comparison, absorption cross section was calculated using parameters from NASA report on high frequency scattering of dielectric disks [9]. Horizontal and vertical polarization were both taken into account. Comparison was done for three frequency values. 1GHz, as low frequency, 4 GHz as mid and critical frequency, and lastly 7 GHz, as high frequency were calculated. 4 GHz is mentioned as critical frequency, because of the restriction in approximation.

The thickness of the dielectric disk is taken as 1 mm, and radius is 7 cm. Angle of incidence is 30^o for calculations. relative dielectric constant is taken as $36 + i13$ that corresponds to a leave with 70% water content.

Table 3.1. Comparison of calculated absorption cross section with NASA report for horizontal polarization.

Frequency	NASA Report	Thesis Model	Error %
1.0 GHz	0.00276	0.0025	9.42
4.0 GHz	0.00318	0.0032	-0.629
7.0 GHz	0.00264	0.0026	1.515

In Table 3.1, three values of absorption cross section of disk is given with frequencies. At 1 GHz, calculated absorption cross section is about 0.0025 and for NASA report, that value is 0.00276. Error is about 9.42 %, that is not a small error. However, if dimensions of the disk are considered, radius of the disk (0.07 m) is much smaller than the wavelength (0.299 m). Therefore, the assumption made in the absorption cross section approximations part is not valid. Results might be improved by another method.

At larger frequencies, for 4 GHz and 7 GHz, error percentage is smaller enough to accept that the calculated results for the model are accurate. At 4 GHz, error is

0.629% and for 7 GHz, error is 1.515 %.

4. SIMULATION

In this chapter, resulting equations for the emissivity of modeled leaves ,branches and trunks of the subject vegetation is simulated using MATLAB program [58]. Emissivity of leaves obtained from the disk shaped dielectric equation that is calculated using physical optics approximation in the previous chapter. For the emissivity of branches and trunks of the vegetation, infinite length approximation is utilized for a cylinder. Randomly oriented disks and cylinders are considered and simulated with specified geometrical and observational parameters given in tables.

4.1. Leaf Model Emissivity Simulations

In this section, leaf model simulation is given. In tables; θ_v, f_v, a_v, ϵ'_v, ϵ''_v and $n\Delta z_v$ represents second parameter in simulations, for example in emissivity versus frequency graph, three values of the angle of incidence is used and it is given in table as θ_v. In Figure 4.1, leaf model that is disk in specified geometry is given. Model is simulated for horizontal and vertical polarizations of the wave.

Different thicknesses and diameters for leaves were selected in simulations. Thick and thin leaves were considered according to the assumption that if the ratio a/δ is smaller or equal to 10, then the leaf is called as thick disk. Otherwise, it is assumed as thin disk.

4.1.1. Emissivity versus Frequency - Horizontal Polarization

Emissivity of leaf simulation with respect to frequency is given for three values of three variables in horizontal polarization. In all, frequency is continuously changed and three curves exist for each variables. Increase in frequency, results in decrease in emissivity in all curves except for the smallest real component of the complex relative permittivity.

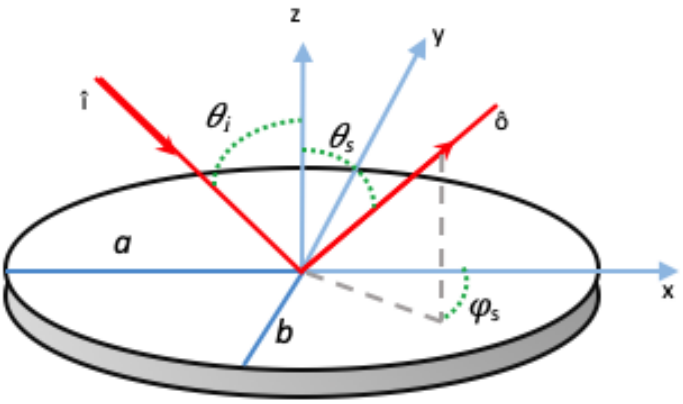

Figure 4.1. Leaf model geometry and vector representations.

In Figure 4.2, frequency was simulated for three radius values. Radius is one of the multipliers in Equation 2.28, therefore larger radius value causes higher emissivity.

Thickness of the leaf has similar effect on emissivity. In Figure 4.3, three curves for thickness (δ) values were given. Thick leaves have larger emissivity, that is also a result from the absorption cross section equation.

Angle of incidence is another critical parameter for emissivity. In Equation 2.7 and Equation 2.4, angle of incidence has direct effect. If the cosine factor in Equation 2.4 is considered, higher angle of incidence causes low emissivity.

Real and imaginary parts of dielectric constant were simulated separately. Real component is not shown at first sight in equations, however the imaginary component is a direct multiplier in absorption cross section. Imaginary part is responsible for the loss of the material, so that the higher value means higher emissivity. In case of the real part, it effects the emissivity indirectly. The smaller real part has higher emissivity in simulation results.

Table 4.1. Plotting parameters for emissivity versus frequency graph of leaf for horizontal polarization.

Parameters	Graph.1	Graph.2	Graph.3	Graph.4	Graph.5
Radius of Leaf (a) (m)	a_v	0.04	0.04	0.04	0.04
Thickness $(\delta)(m)$	0.002	δ_v	0.002	0.002	0.002
Angle of Incidence	30	30	θ_v	30	30
Real Part (ϵ_r')	18.3	18.3	18.3	ϵ_v'	18.3
Imaginary Part (ϵ_r'')	7.0	7.0	7.0	7.0	ϵ_v''
# of Scatterers $(n\Delta z)$	1000	1000	1000	1000	1000

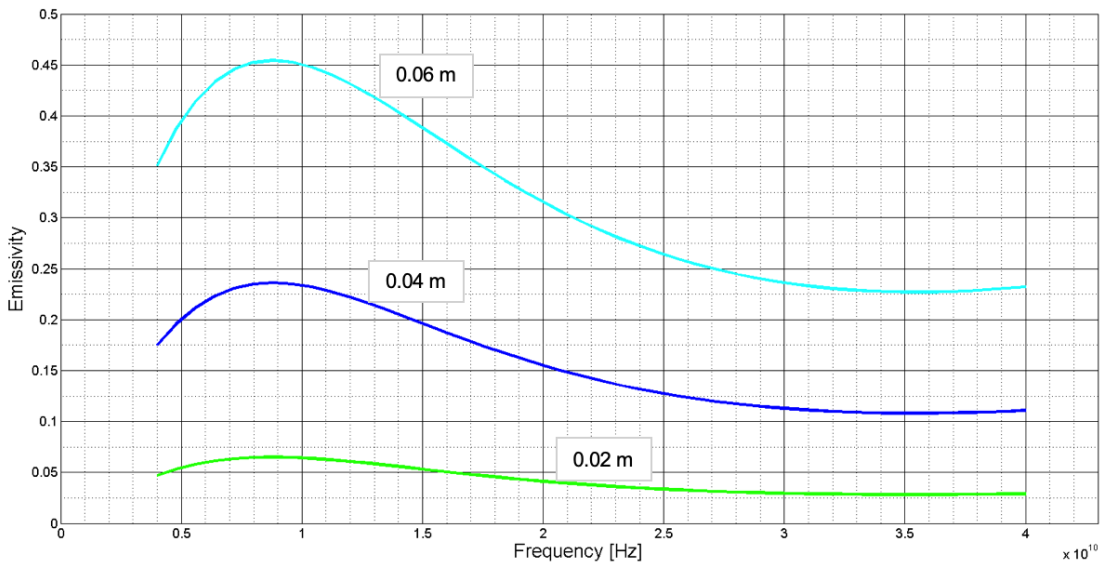

Figure 4.2. Emissivity versus frequency graph for leaves with three values of leaf radius for horizontal polarization.

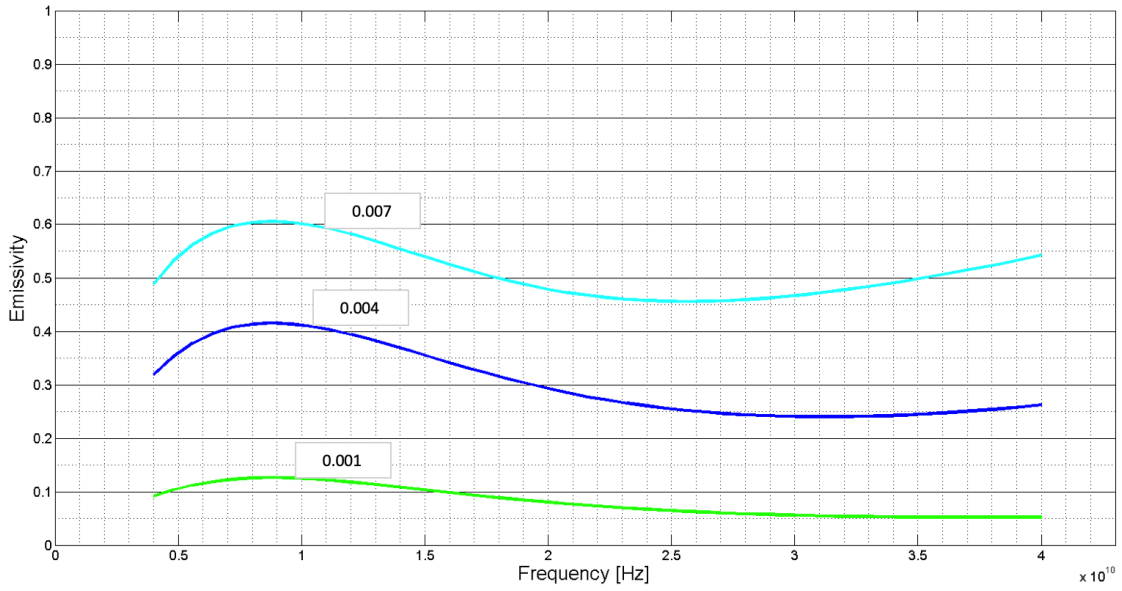

Figure 4.3. Emissivity versus frequency graph for leaves with three values of leaf thickness for horizontal polarization.

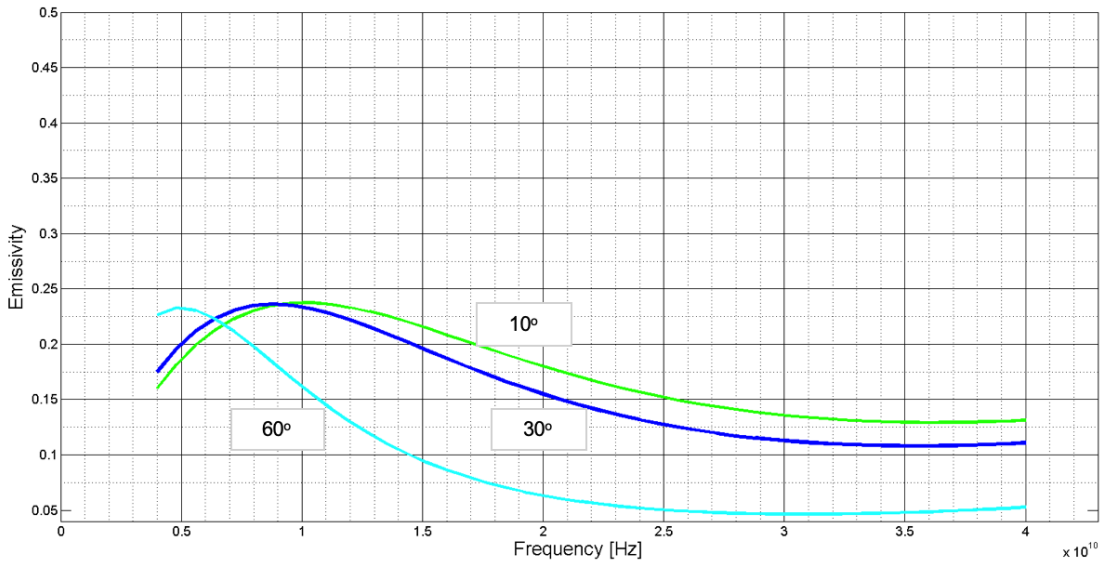

Figure 4.4. Emissivity versus frequency graph for leaves with three values of angle of incidence for horizontal polarization.

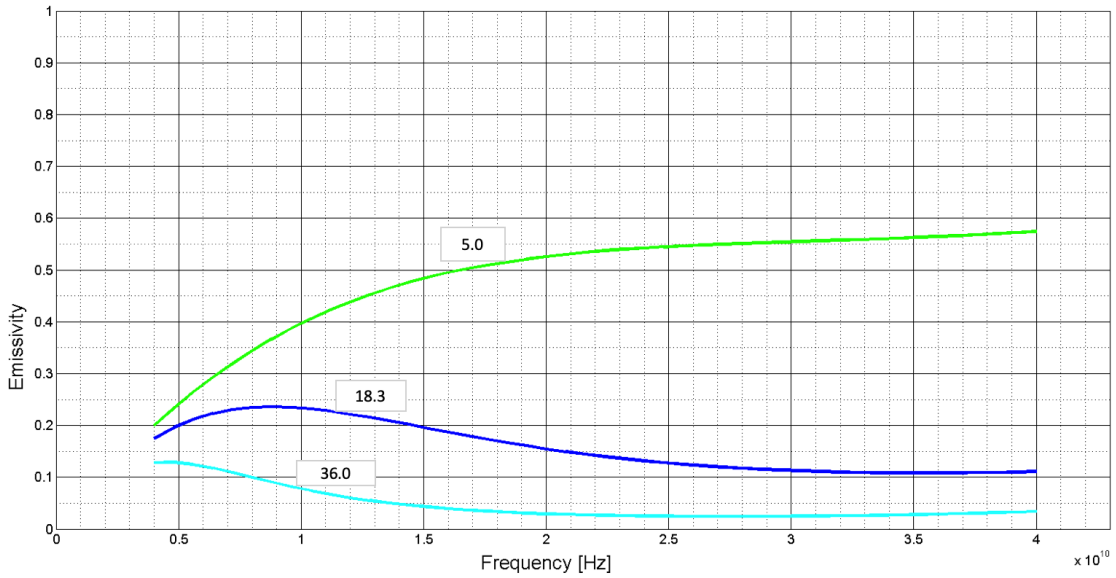

Figure 4.5. Emissivity versus frequency graph for leaves with three values of ϵ_r' for horizontal polarization.

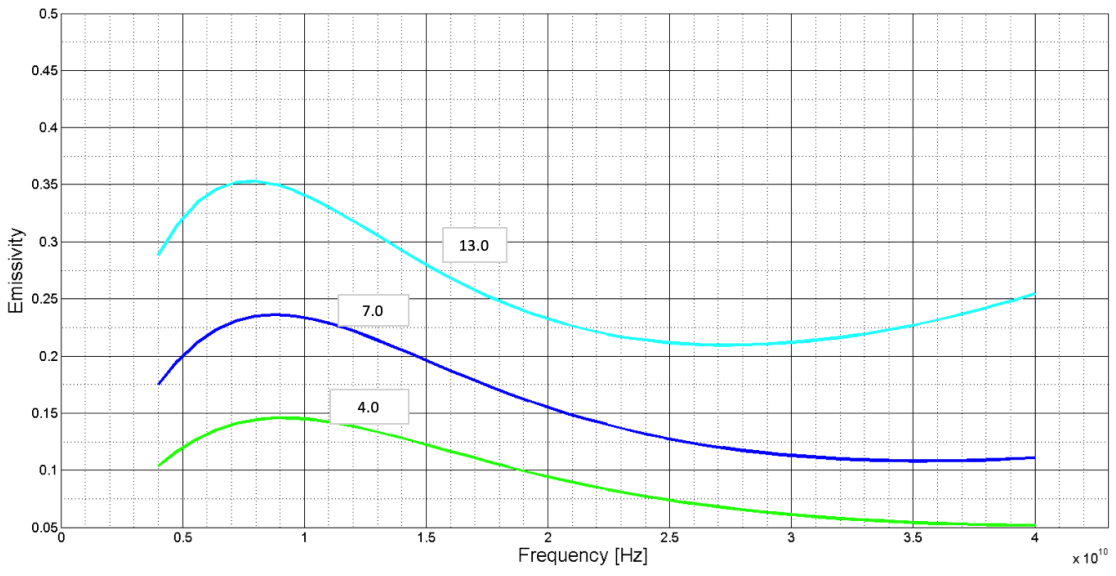

Figure 4.6. Emissivity versus frequency graph for leaves with three values of ϵ_r'' for horizontal polarization.

4.1.2. Emissivity versus Angle of Incidence - Horizontal Polarization

Emissivity versus angle of incidence simulations are given in this subsection. Emissivity decreases with increase in angle of incidence in curves generally. Angle of incidence takes part directly in Equation 2.4. If the angle between incoming wave and normal vector is large, transmission factor is higher. Transmission effects emissivity inversely.

In Figure 4.7, emissivity is simulated with three leaf radius value. Similar to frequency simulation, higher radius has higher emissivity value. After some region, stable emissivity decreases. As for the thickness (δ), thicker leaf has higher emissivity value. Absorbed power in Equation 2.8 increases with increasing leaf thickness.

Table 4.2. Plotting parameters for emissivity versus angle of incidence graph of leaf for horizontal polarization.

Parameters	Graph.1	Graph.2	Graph.3	Graph.4	Graph.5
Radius of Leaf (a) (m)	a_v	0.04	0.04	0.04	0.04
Thickness $(\delta)(m)$	0.002	δ_v	0.002	0.002	0.002
Frequency (GHz)	10	10	f_v	10	10
Real Part (ϵ_r')	18.3	18.3	18.3	ϵ_v'	18.3
Imaginary Part (ϵ_r'')	7.0	7.0	7.0	7.0	ϵ_v''
# of Scatterers $(n\Delta z)$	1000	1000	1000	1000	1000

Figure 4.9 displays three curves created with 7 GHz, 10 GHz, and 20 GHz frequencies. In 7 GHz frequency, emissivity stays almost constant. 10 GHz and 7 GHz intersects at 35^o angle. The reason for that, increase in frequency does not directly result in a decrease in emissivity. For higher frequencies, as in 20 GHz, emissivity is much smaller.

Complex relative permittivity was observed for also angle of incidence simulation. As it was mentioned before, imaginary component is direct multiplier and effect on emissivity is obvious. However, real component takes part in β_z in Equation 2.14. For the smallest, that is 5, emissivity increases with a small slope. Larger real parts has lower emissivity values, and after some region emissivity decreases.

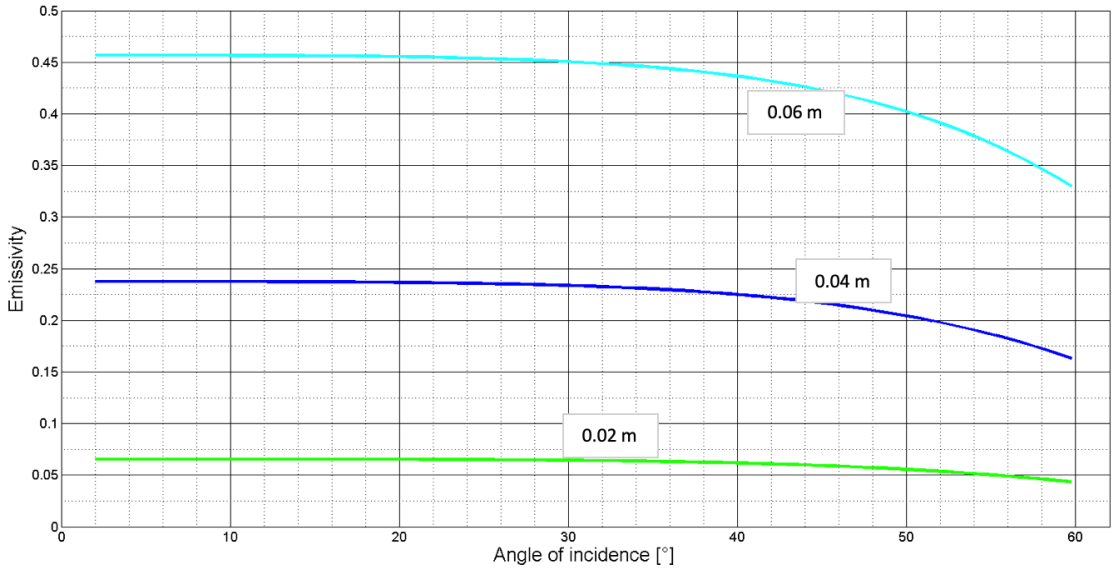

Figure 4.7. Emissivity versus angle of incidence graph for leaves with three values of leaf radius for horizontal polarization.

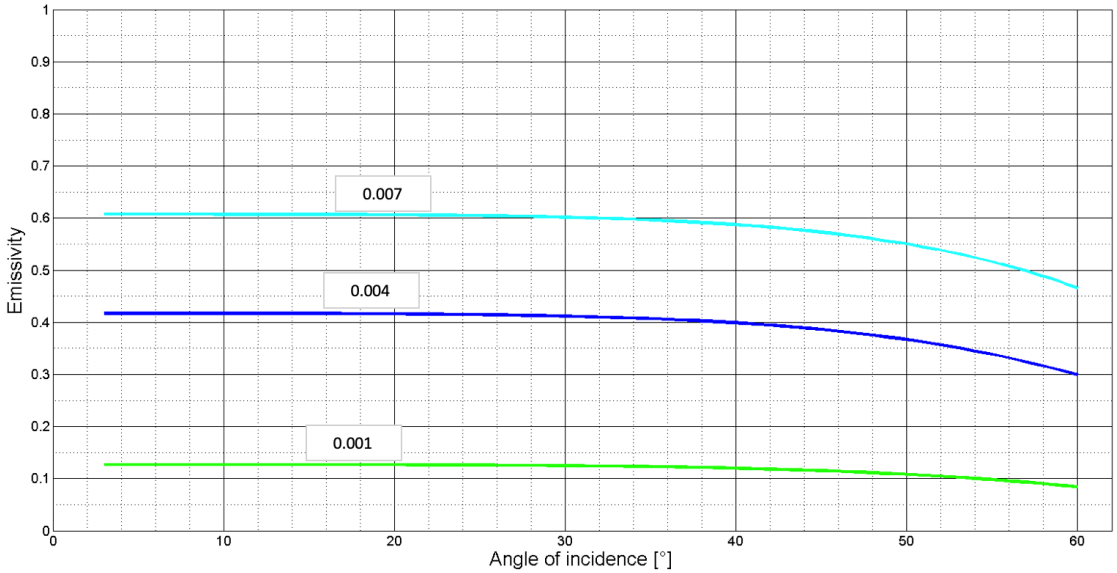

Figure 4.8. Emissivity versus angle of incidence graph for leaves with three values of leaf thickness for horizontal polarization.

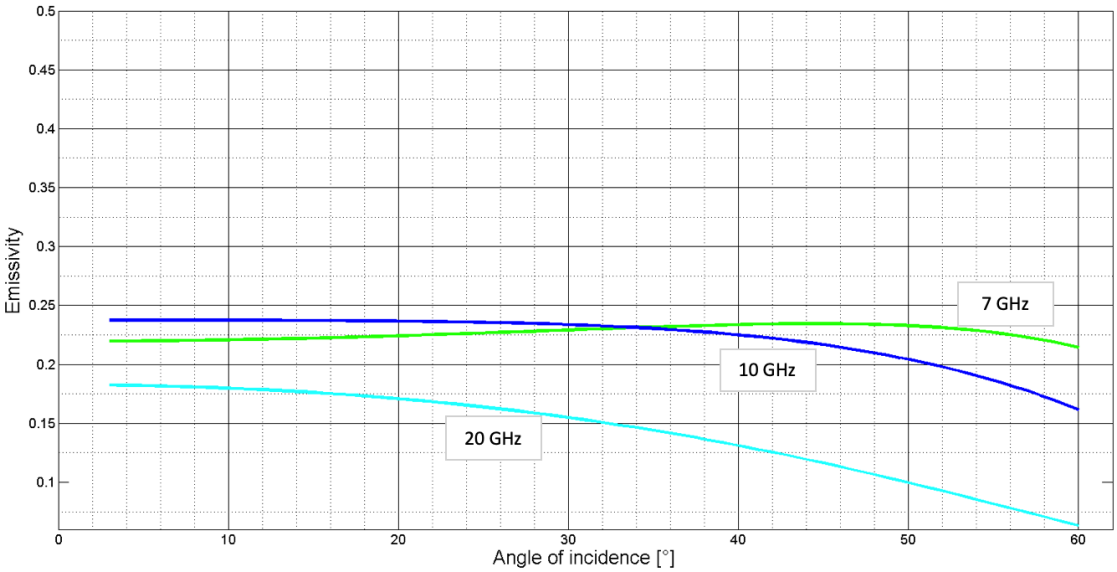

Figure 4.9. Emissivity versus angle of incidence graph for leaves with three values of frequency for horizontal polarization.

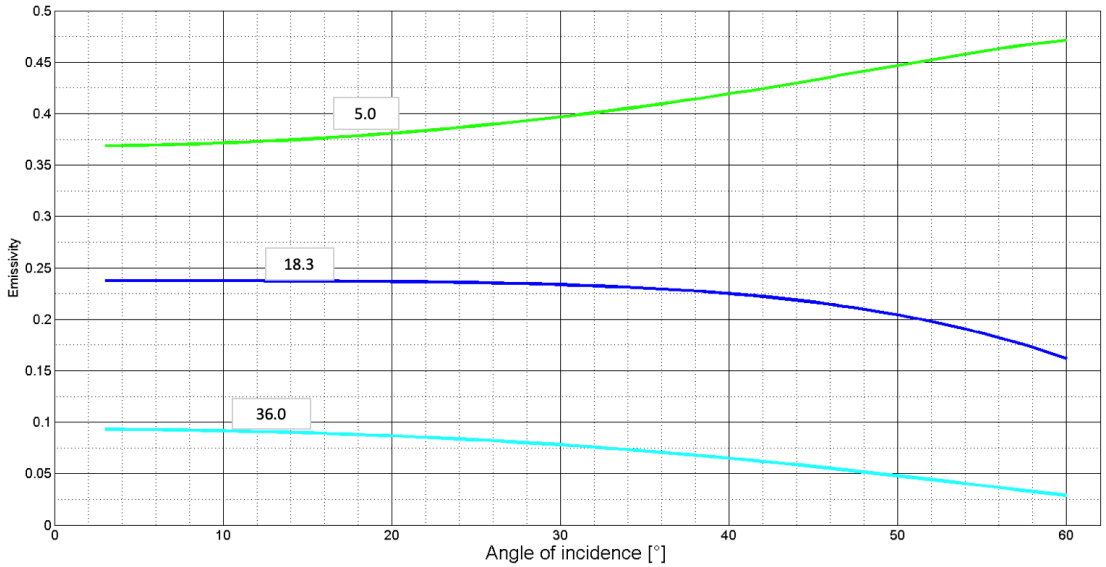

Figure 4.10. Emissivity versus angle of incidence graph for leaves with three values of ϵ_r' for horizontal polarization.

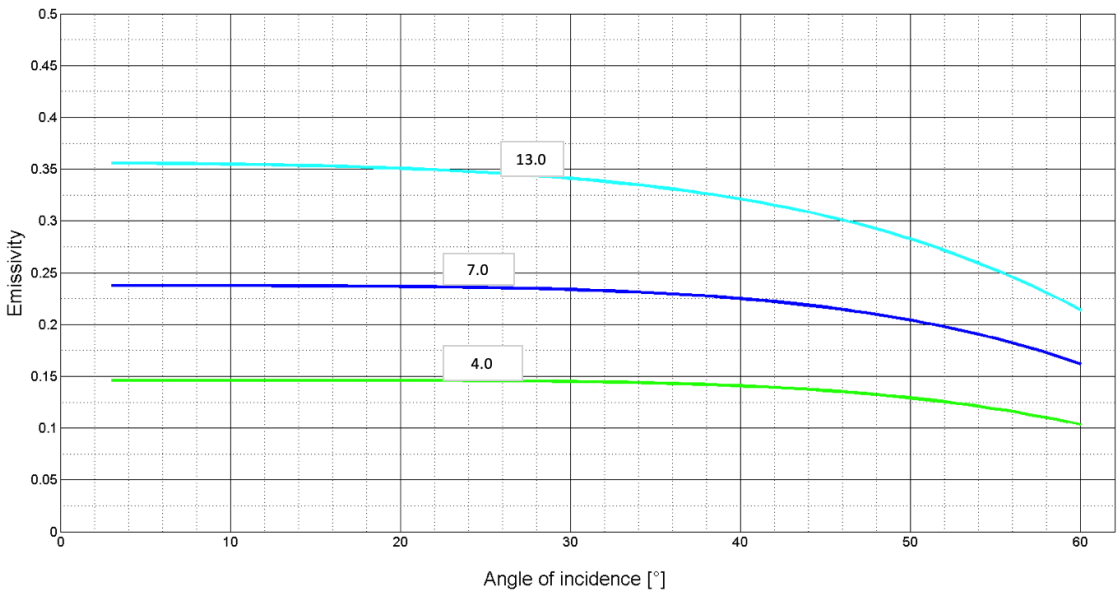

Figure 4.11. Emissivity versus angle of incidence graph for leaves with three values of ϵ_r'' for horizontal polarization.

4.1.3. Emissivity versus Frequency - Vertical Polarization

Emissivity of leaf simulation with respect to frequency is given for three values of three variables in vertical polarization. In all, frequency is continuously changed and three curves exist for each variables. Increase in frequency, results in increase in emissivity in all curves.

In Figure 4.12, frequency was simulated for three radius values. Radius is one of the multipliers in Equation 2.28, therefore larger radius value causes higher emissivity.

Thickness of the leaf has similar effect on emissivity, meanly increase in thickness increases emissivity. In Figure 4.13, three curves for thickness (δ) values were given. Thick leaves have larger emissivity, that is also a result from the absorption cross section equation.

Table 4.3. Plotting parameters for emissivity versus frequency graph of leaf for vertical polarization.

Parameters	Graph.1	Graph.2	Graph.3	Graph.4	Graph.5
Radius of Leaf (a) (m)	a_v	0.04	0.04	0.04	0.04
Thickness $(\delta)(m)$	0.002	δ_v	0.002	0.002	0.002
Angle of Incidence	30	30	θ_v	30	30
Real Part (ϵ_r')	18.3	18.3	18.3	ϵ_v'	18.3
Imaginary Part (ϵ_r'')	7.0	7.0	7.0	7.0	ϵ_v''
# of Scatterers $(n\Delta z)$	1000	1000	1000	1000	1000

Angle of incidence is another parameter. At low frequencies, smaller than 15 GHz, change in angle is not effective on emissivity. For higher frequencies, increasing angle increases emissivity.

Real and imaginary parts of dielectric constant were simulated separately. Real component is not shown at first sight in equations, however the imaginary component is a direct multiplier in absorption cross section. Imaginary part is responsible for the loss of the material, so that the higher value means higher emissivity. In case of the real part, it effects the emissivity indirectly. The smaller real part has higher emissivity in simulation results.

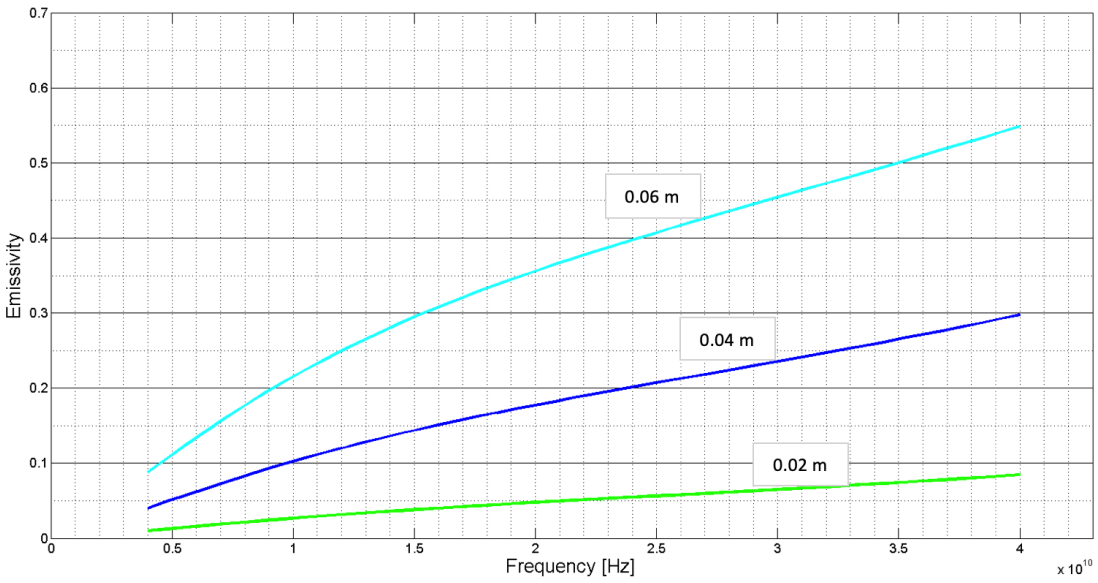

Figure 4.12. Emissivity versus frequency graph for leaves with three values of leaf radius for vertical polarization.

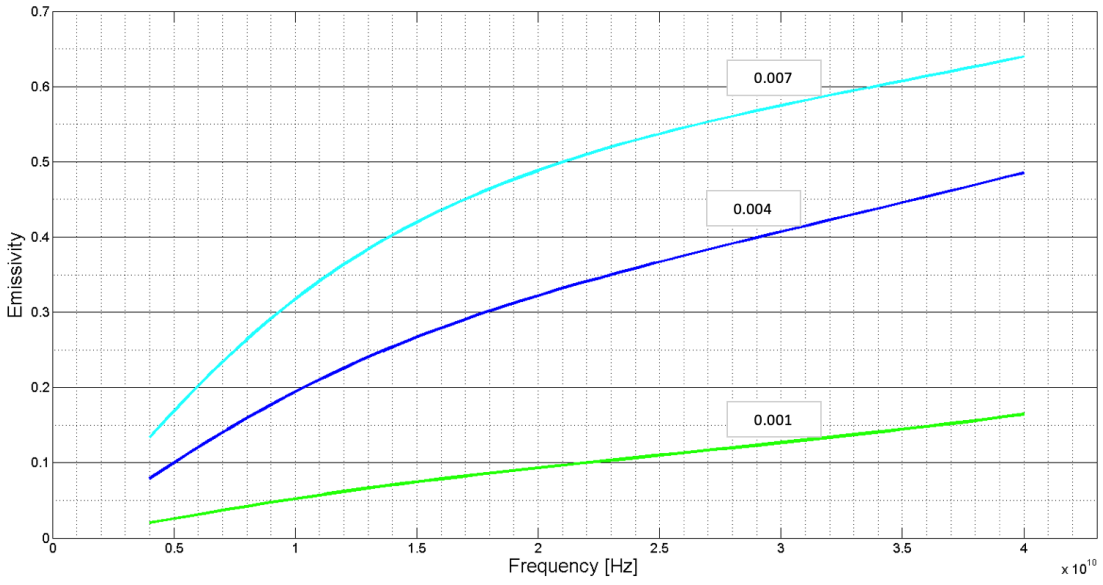

Figure 4.13. Emissivity versus frequency graph for leaves with three values of leaf thickness for vertical polarization.

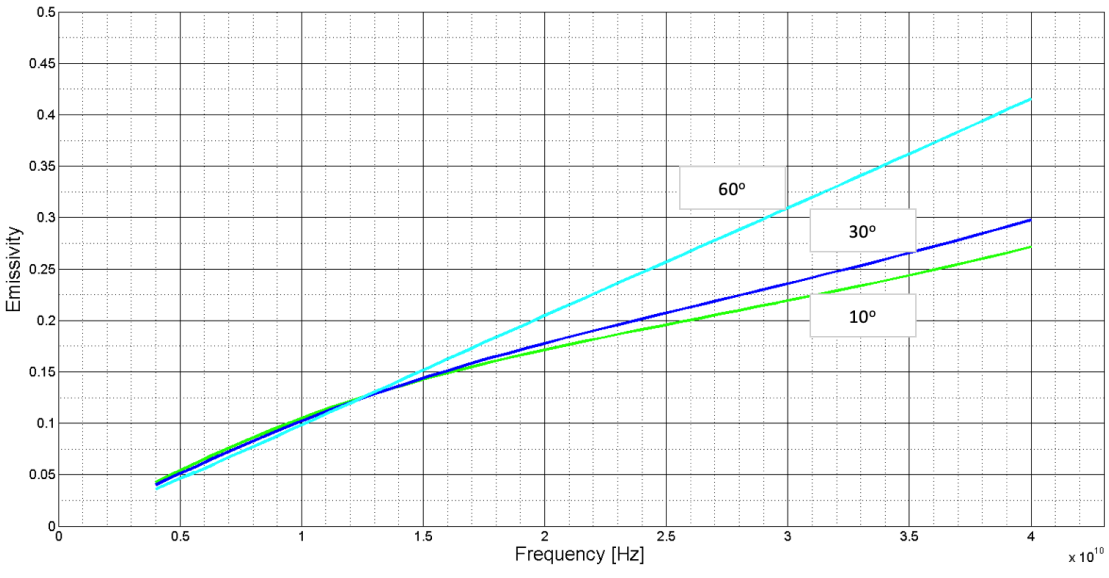

Figure 4.14. Emissivity versus frequency graph for leaves with three values of angle of incidence for vertical polarization.

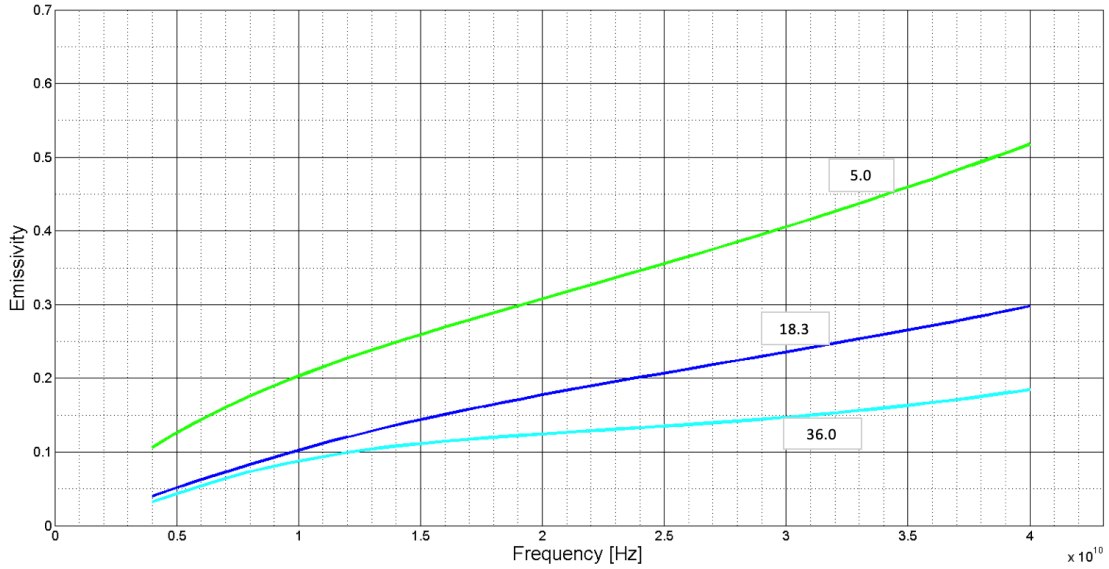

Figure 4.15. Emissivity versus frequency graph for leaves with three values of ϵ_r' for vertical polarization.

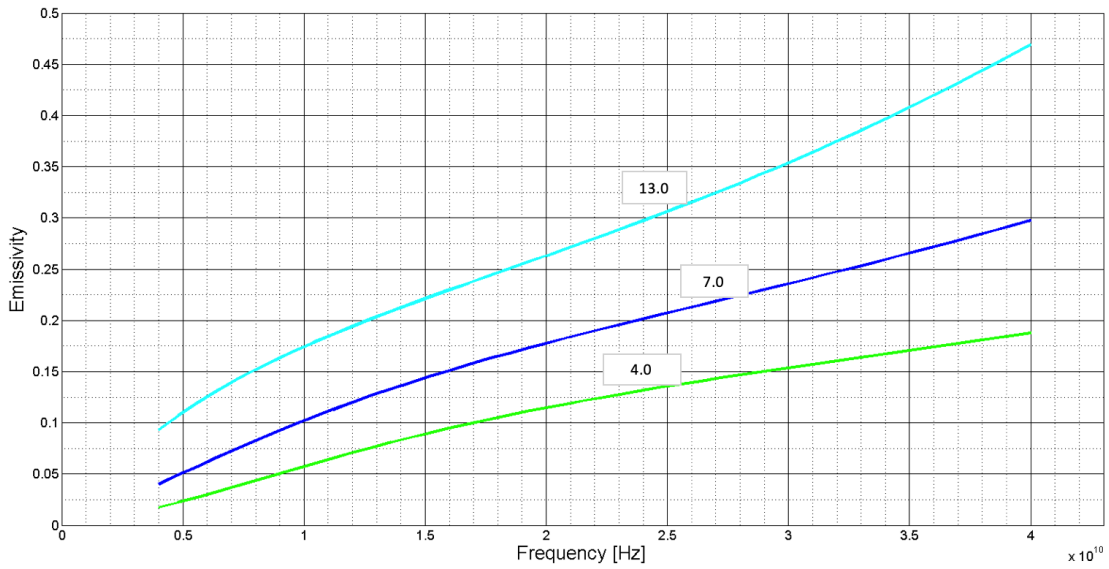

Figure 4.16. Emissivity versus frequency graph for leaves with three values of ϵ_r'' for vertical polarization.

4.1.4. Emissivity versus Angle of Incidence - Vertical Polarization

Emissivity versus angle of incidence simulations for vertical polarization are given in this subsection. Emissivity stays almost stable with increase in angle of incidence in curves. Vertical polarization changes the effect of angle of incidence on internal electric field and absorption cross section.

In Figure 4.17, emissivity is simulated with three leaf radius value. Similar to frequency simulation, higher radius has higher emissivity value. As for the thickness (δ), thicker leaf has higher emissivity value. Absorbed power in Equation 2.8 increases with increasing leaf thickness.

Table 4.4. Plotting parameters for emissivity versus angle of incidence graph of leaf for vertical polarization.

Parameters	Graph.1	Graph.2	Graph.3	Graph.4	Graph.5
Radius of Leaf (a) (m)	a_v	0.04	0.04	0.04	0.04
Thickness $(\delta)(m)$	0.002	δ_v	0.002	0.002	0.002
Frequency (GHz)	10	10	f_v	10	10
Real Part (ϵ_r')	18.3	18.3	18.3	ϵ_v'	18.3
Imaginary Part (ϵ_r'')	7.0	7.0	7.0	7.0	ϵ_v''
# of Scatterers $(n\Delta z)$	1000	1000	1000	1000	1000

Figure 4.19 displays three curves created with 7 GHz, 10 GHz, and 20 GHz frequencies. At these frequency values, emissivity stays almost constant with increasing angle of incidence. Higher frequency results in higher emissivity value.

Complex relative permittivity was observed for also angle of incidence simulation. As it was mentioned before, imaginary component is direct multiplier and therefore larger value increases emissivity. However, real component takes part in β_z in Equation 2.14. For all of real part values, emissivity stays constant. Larger real parts has lower

emissivity values, and after some region emissivity decreases.

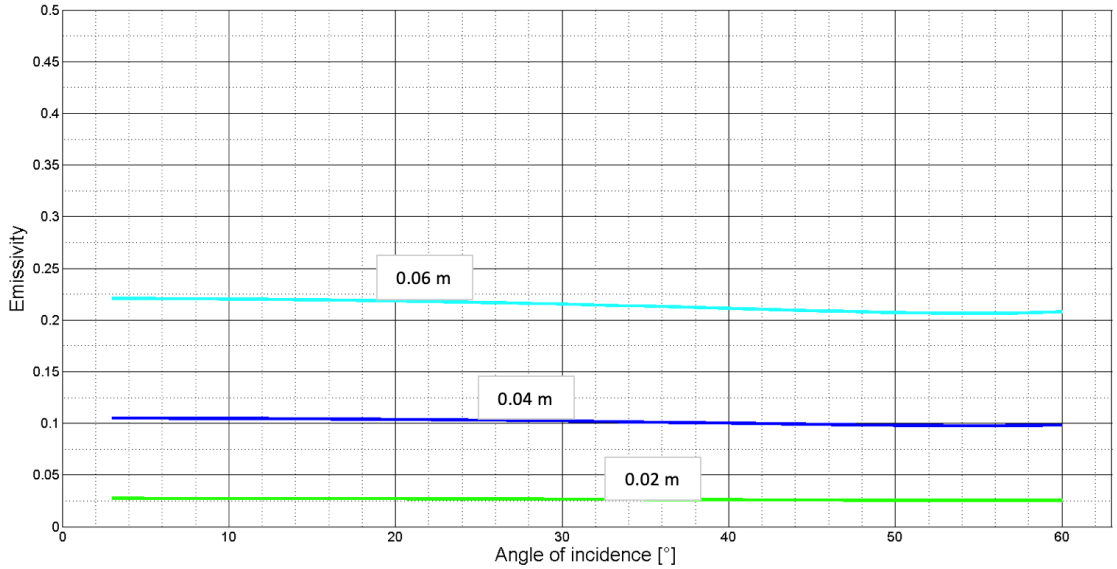

Figure 4.17. Emissivity versus angle of incidence graph for leaves with three values of leaf radius for vertical polarization.

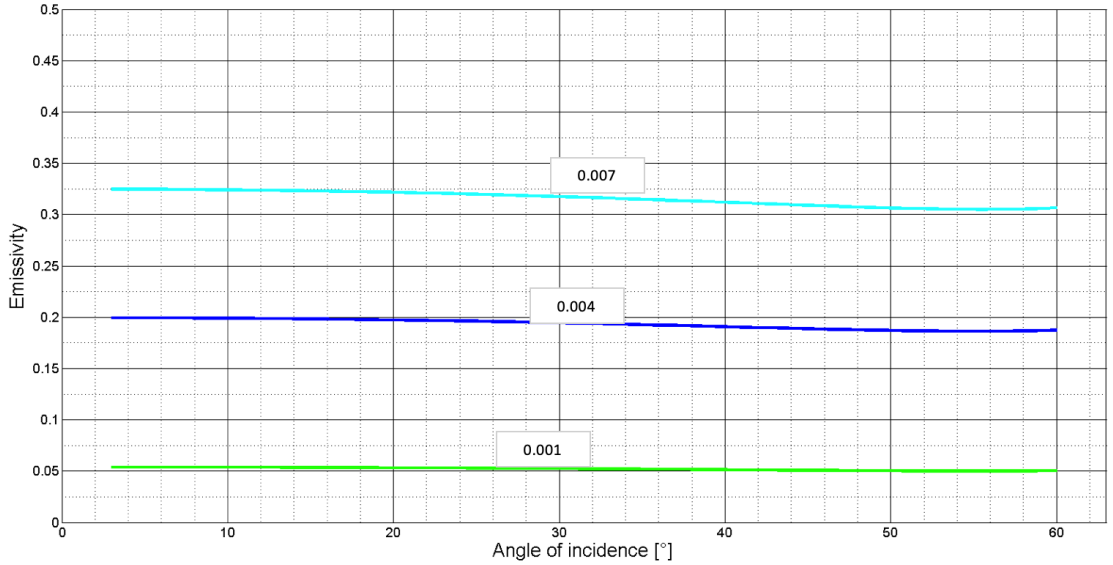

Figure 4.18. Emissivity versus angle of incidence graph for leaves with three values of leaf thickness for vertical polarization.

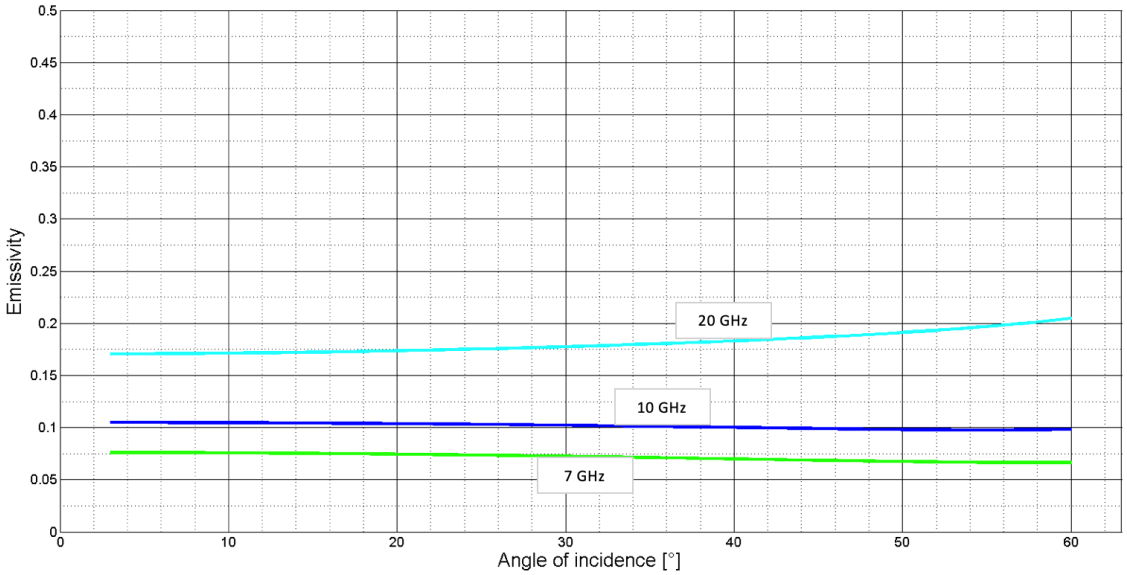

Figure 4.19. Emissivity versus angle of incidence graph for leaves with three values of frequency for vertical polarization.

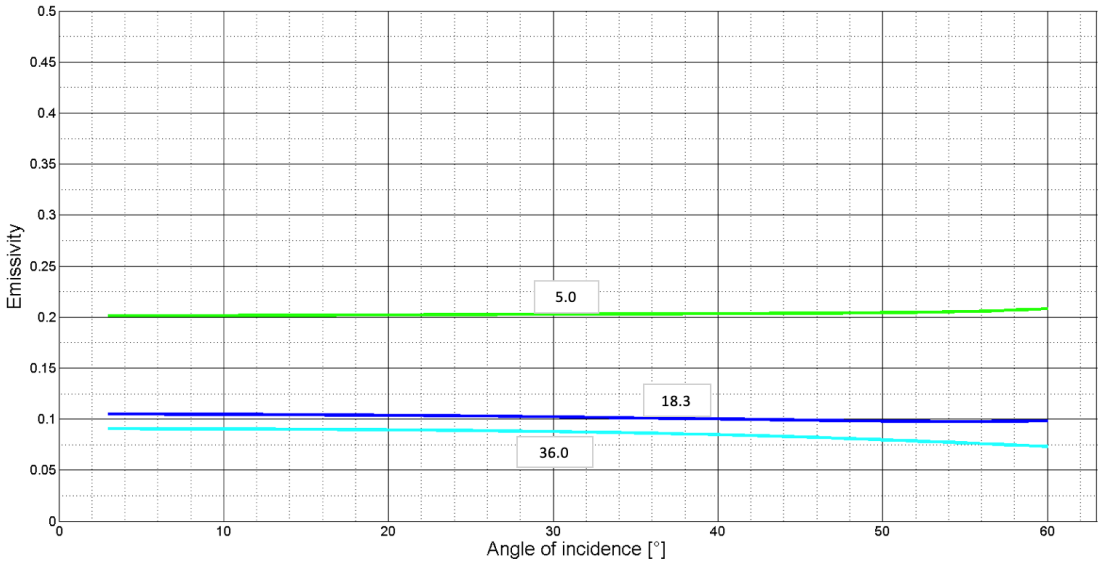

Figure 4.20. Emissivity versus angle of incidence graph for leaves with three values of ϵ_r' for vertical polarization.

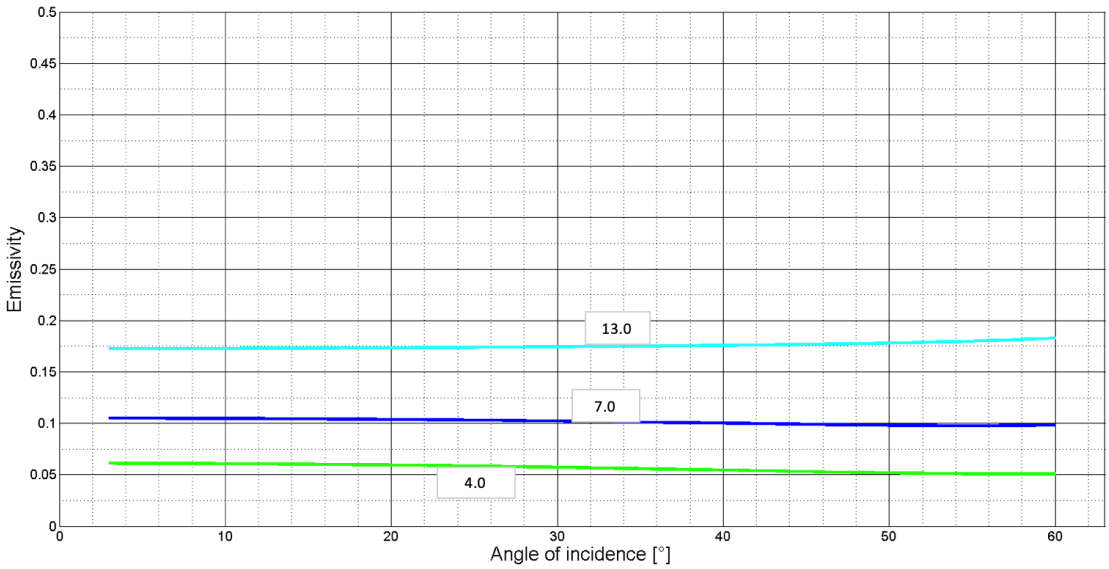

Figure 4.21. Emissivity versus angle of incidence graph for leaves with three values of ϵ_r'' for vertical polarization.

4.2. Branch and Trunk Model Emissivity Simulations

In this section, branches and trunks of vegetation are simulated for continuously changing frequency, angle of incidence, and geometry of cylinder model. Horizontal and vertical polarizations are considered in separated graphs. Cylinder model is given in Figure 4.22 with vector representations.

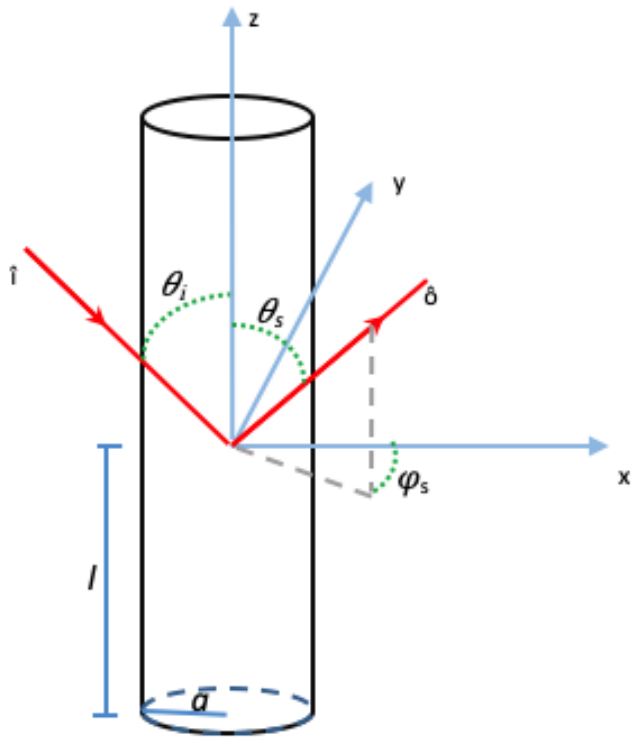

Figure 4.22. Leaf model geometry and vector representations.

4.2.1. Emissivity versus Frequency - Horizontal Polarization

Emissivity of branch and trunks are simulated with respect to changing frequency. To some point, emissivity increases; however at higher frequencies emissivity decreases. Together with the changing frequency, cylinder radius, cylinder length, angle of incidence and complex relative permittivity is simulated to obtain specific relations between pairs.

In the first graph, Figure 4.23, effect of radius and length was displayed. Thin branches have lower emissivity and trunks have higher, as it is expected from the Equation 2.51. Because of the volume integral of wave transformation equation, length and radius are direct multipliers. As for the angle of incidence curves are given in Figure 4.24. Cylinder geometry is different than the disk geometry. Increasing angle effect emissivity in good direction. 60^o angle causes better absorption and therefore effect of cosine factor in Equation 2.4 is smaller.

Table 4.5. Plotting parameters of emissivity versus frequency graph of branch and trunk for horizontal polarization.

Parameters	Graph.1	Graph.2	Graph.3	Graph.4
Radius of Cylinder (a) (m)	a_v	0.02	0.02	0.02
Cylinder Length $(2l)$ (m)	l_v	1.00	1.00	1.00
Angle of Incidence	30^o	θ_v	30^o	30^o
Real Part (ϵ_r')	18.7	18.7	ϵ_v'	15
Imaginary Part (ϵ_r'')	7.0	7.0	7.0	ϵ_v''
# of Scatterers $(n\Delta z)$	32	32	64	64

Equations of electric field components for three axes, which are in Equation 2.31, Equation 2.32 and Equation 2.33 provide that dielectric constant directly effects internal electric field. Internal electric field constitutes the absorption cross section and emissivity. Real and imaginary parts of dielectric constant was investigated in separate graphs similarly. Imaginary part is again a multiplier of the absorption cross section. Dielectric constant also takes place in coefficient equations that come from boundary conditions solution. For both components, high value causes higher emissivity.

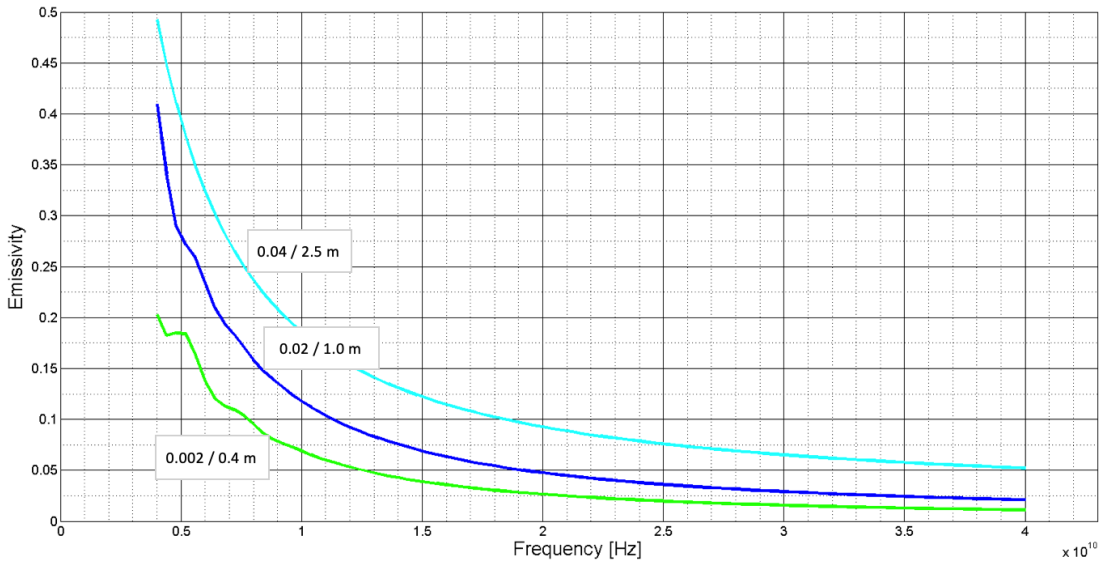

Figure 4.23. Emissivity versus frequency graph of branches and trunks with three values of cylinder length and radius for horizontal polarization.

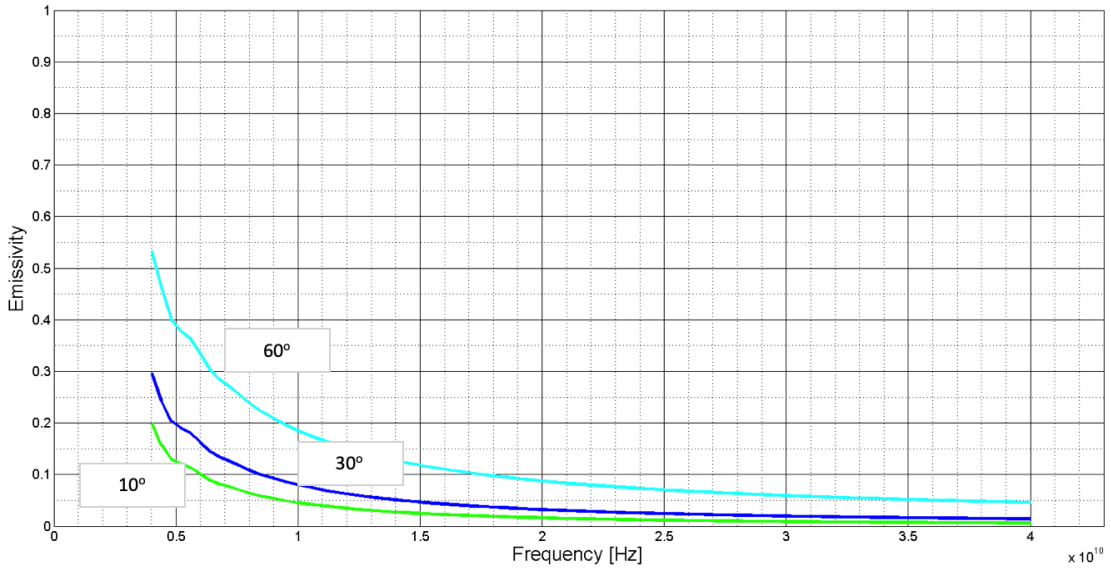

Figure 4.24. Emissivity versus frequency graph of branches and trunks with three values of angle of incidence for horizontal polarization.

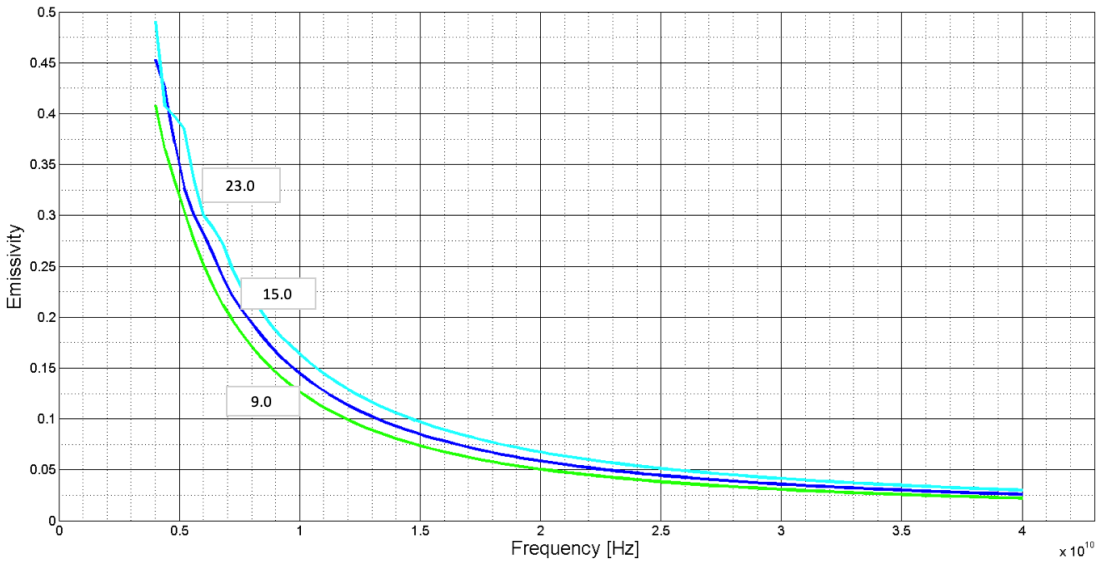

Figure 4.25. Emissivity versus frequency graph of branches and trunks with three values of ϵ_r' for horizontal polarization.

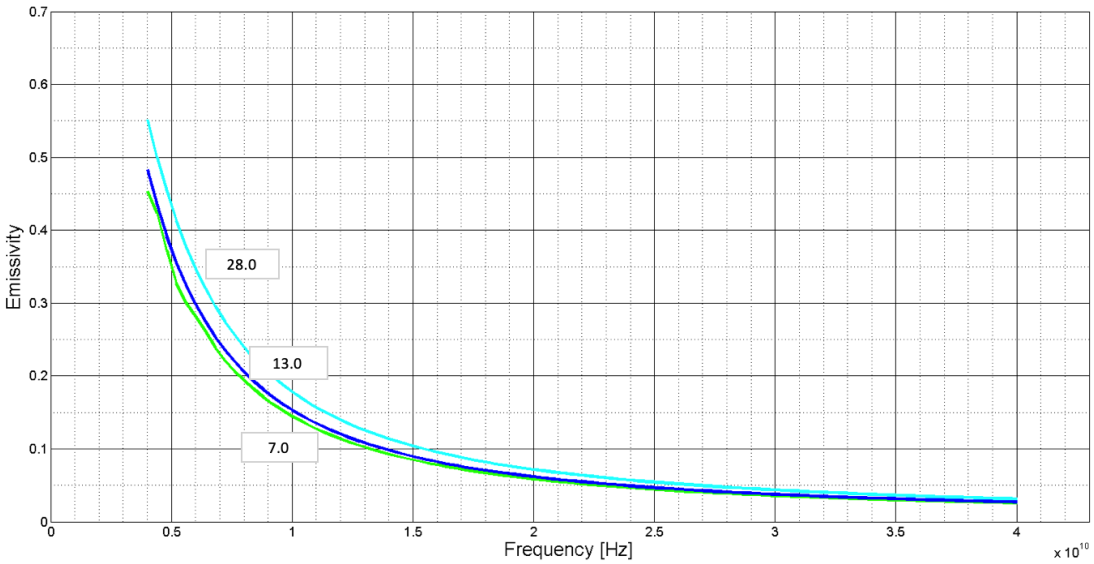

Figure 4.26. Emissivity versus frequency graph of branches and trunks with three values of ϵ_r'' for horizontal polarization.

4.2.2. Emissivity versus Angle of Incidence - Horizontal Polarization

Incident angle is considered as a second parameter in emissivity simulation of branch model. With different dimensions, frequencies and dielectric constants three graph was formed. The obvious effect of angle of incidence is an increase in emissivity. The geometry and therefore the effect on emissivity is different than leaf model.

In dimensional change, angle of incidence effect emissivity values of geometrically similar branches. At 50^o, two curves intersect. Trunk has higher emissivity than others, because of higher absorption. Incidence angle effects emissivity and absorption cross section separately. Dominant effect of geometry changes inversely with the change in incidence angle.

Table 4.6. Plotting parameters of emissivity versus angle of incidence graph of branch and trunk for horizontal polarization.

Parameters	Graph.1	Graph.2	Graph.3	Graph.4
Radius of Leaf (a) (m)	a_v	0.02	0.02	0.02
Cylinder Length $(2l)$ (m)	l_v	1.00	1.00	1.00
Frequency (GHz)	10	f_v	10	10
Real Part (ϵ_r')	18.7	18.7	ϵ_v'	18.7
Imaginary Part (ϵ_r'')	7.0	7.0	7.0	ϵ_v''
# of Scatterers $(n\Delta z)$	32	32	64	64

Frequency is another factor that influences electric field inside the object. Wavelength λ_i component in Equation 2.31, Equation 2.32, and Equation 2.33 provides that internal electric field has quite dependence on frequency. As frequency increases emissivity decreases in simulated graphs. In Figure 4.29 and Figure 4.30, real and imaginary component simulations are given. Similar to frequency simulation, larger values of real and imaginary parts result in higher emissivity values.

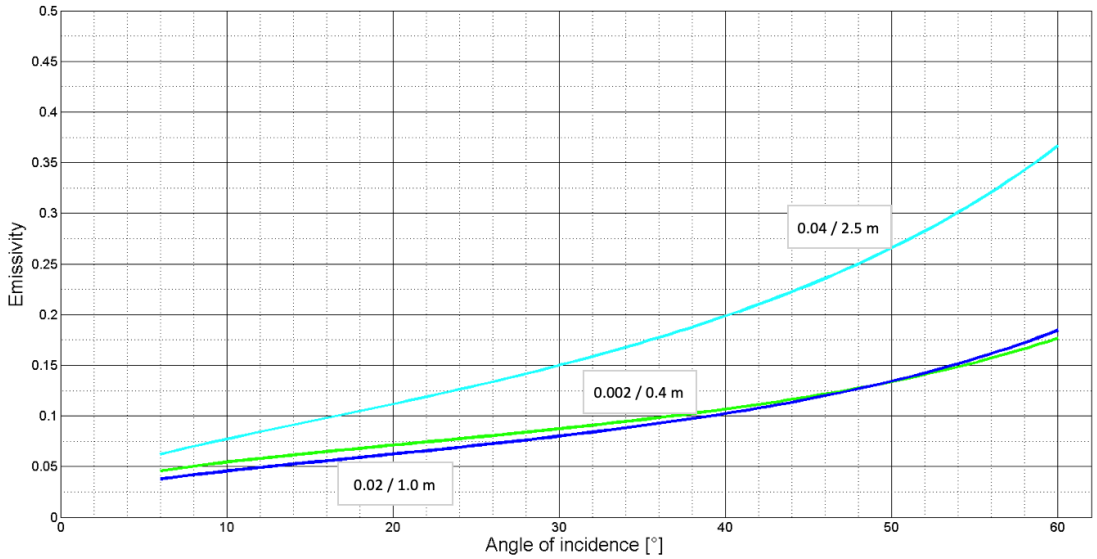

Figure 4.27. Emissivity versus angle of incidence graph of branches and trunks with three values of cylinder length and radius for horizontal polarization.

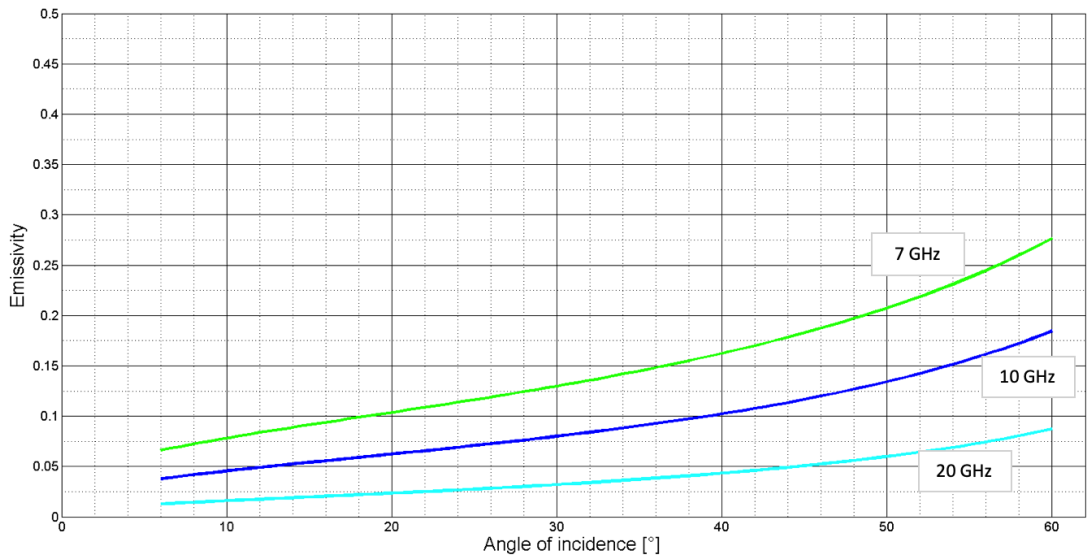

Figure 4.28. Emissivity versus angle of incidence graph of branches and trunks with three values of frequency for horizontal polarization.

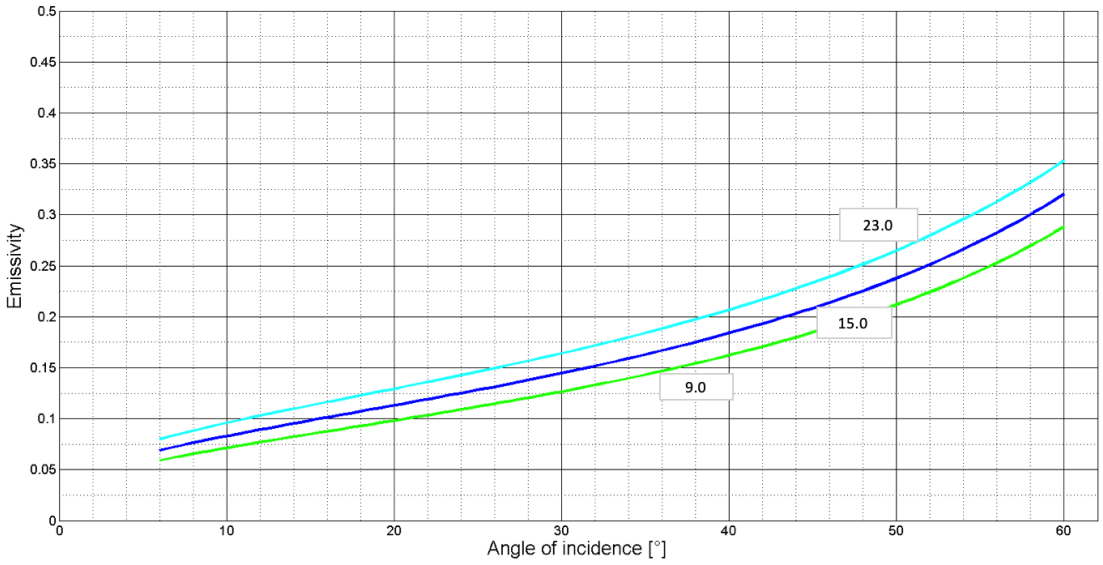

Figure 4.29. Emissivity versus angle of incidence graph of branches and trunks with three values of ϵ_r' for horizontal polarization.

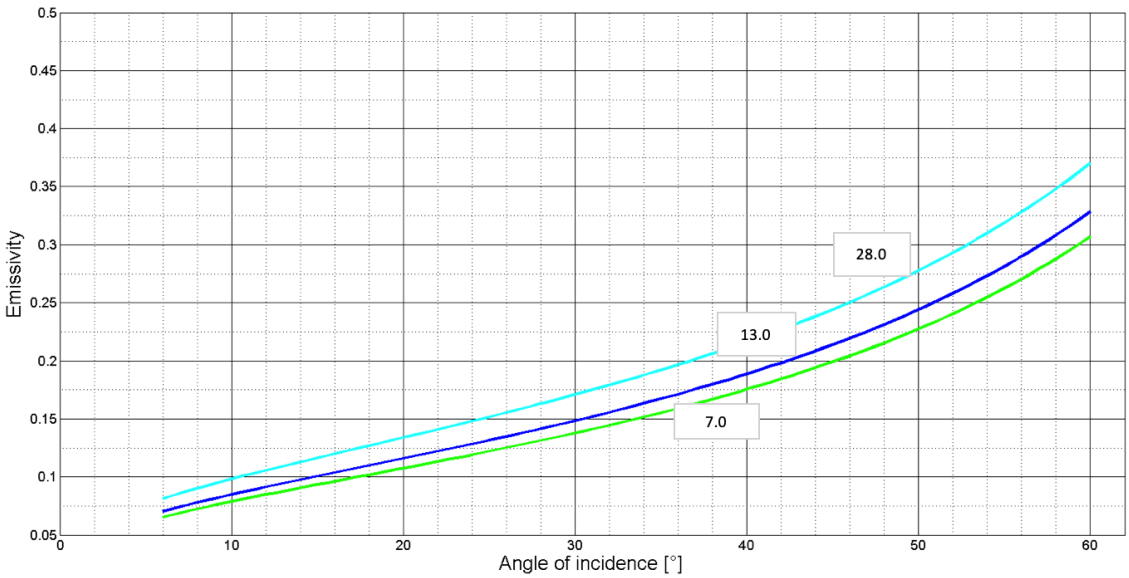

Figure 4.30. Emissivity versus angle of incidence graph of branches and trunks with three values of ϵ_r'' for horizontal polarization.

4.2.3. Emissivity versus Frequency - Vertical Polarization

Emissivity of branch and trunks are simulated with respect to changing frequency. Vertical polarization results are close to horizontal polarization.

In the first graph, Figure 4.31, effect of radius and length was displayed. Thin branches have lower emissivity and trunks have higher, as it is expected from the Equation 2.51. Length and radius are direct multipliers. Angle of incidence curves with changing frequency are given in Figure 4.32. Cylinder geometry is different than the disk geometry, therefore it has different results than disk model simulation. Increasing angle effect emissivity in good direction. 60^o angle causes better absorption and therefore effect of cosine factor in Equation 2.4 is smaller.

Table 4.7. Plotting parameters of emissivity versus frequency graph of branch and trunk for vertical polarization.

Parameters	Graph.1	Graph.2	Graph.3	Graph.4
Radius of Cylinder (a) (m)	a_v	0.02	0.02	0.02
Cylinder Length $(2l)$ (m)	l_v	1.00	1.00	1.00
Angle of Incidence	30^o	θ_v	30^o	30^o
Real Part (ϵ_r')	18.7	18.7	ϵ_v'	15
Imaginary Part (ϵ_r'')	7.0	7.0	7.0	ϵ_v''
# of Scatterers $(n\Delta z)$	32	32	64	64

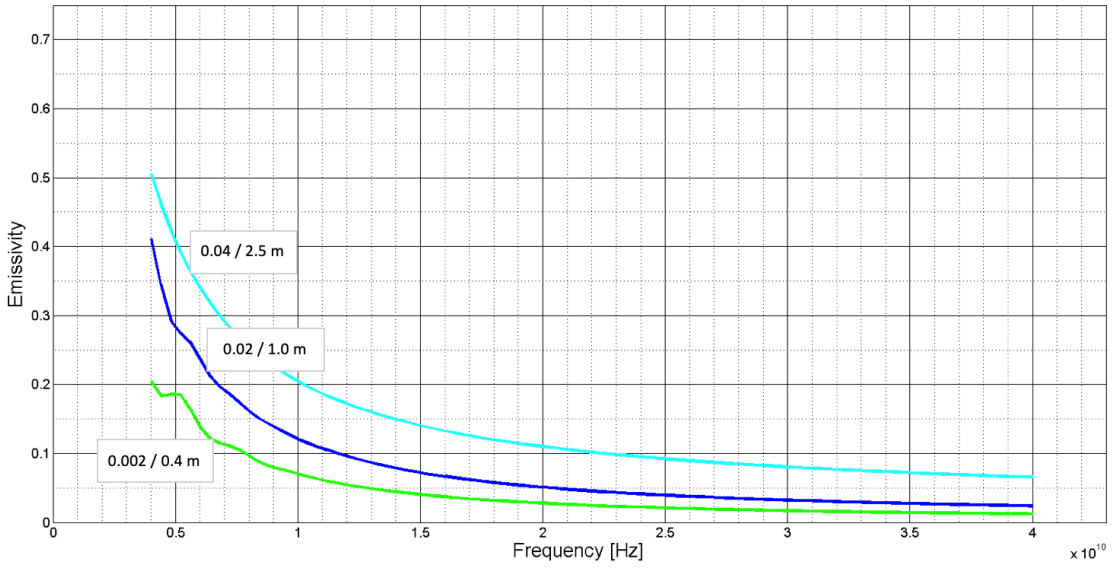

Figure 4.31. Emissivity versus frequency graph of branches and trunks with three values of cylinder length and radius for vertical polarization.

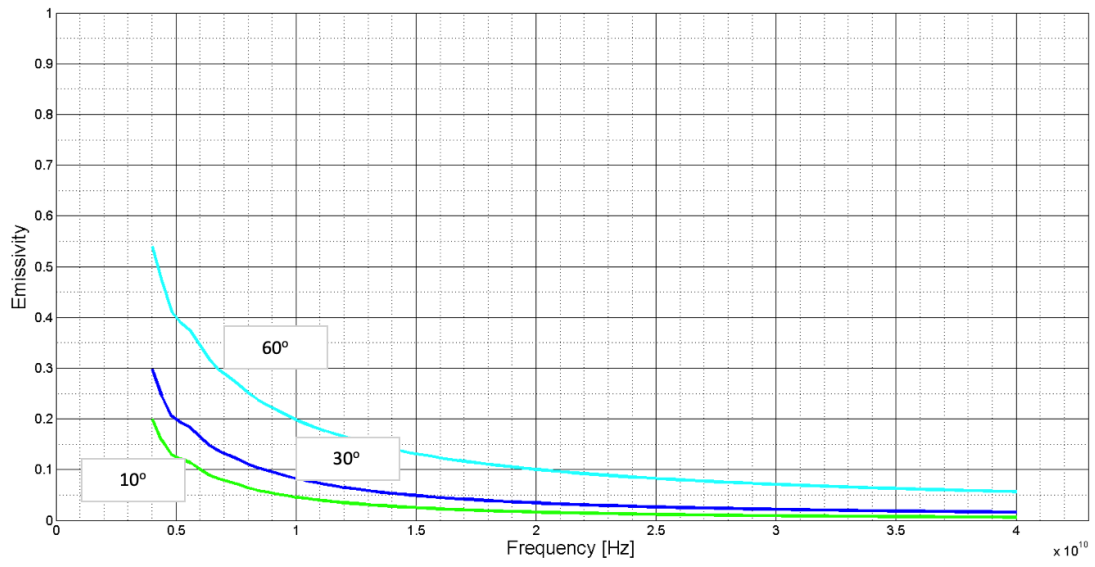

Figure 4.32. Emissivity versus frequency graph of branches and trunks with three values of angle of incidence for vertical polarization.

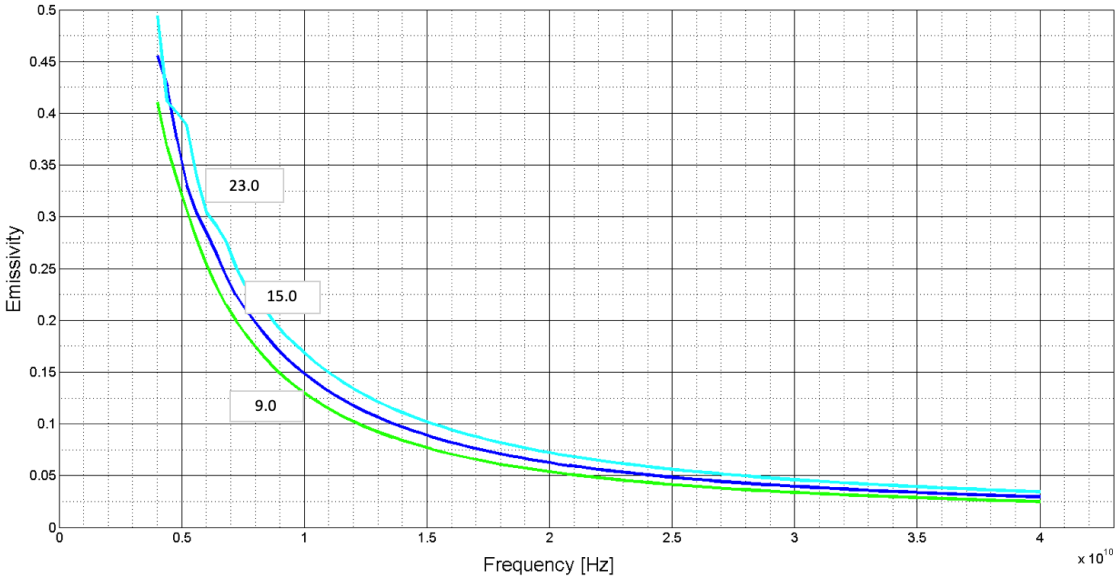

Figure 4.33. Emissivity versus frequency graph of branches and trunks with three values of ϵ_r' for vertical polarization.

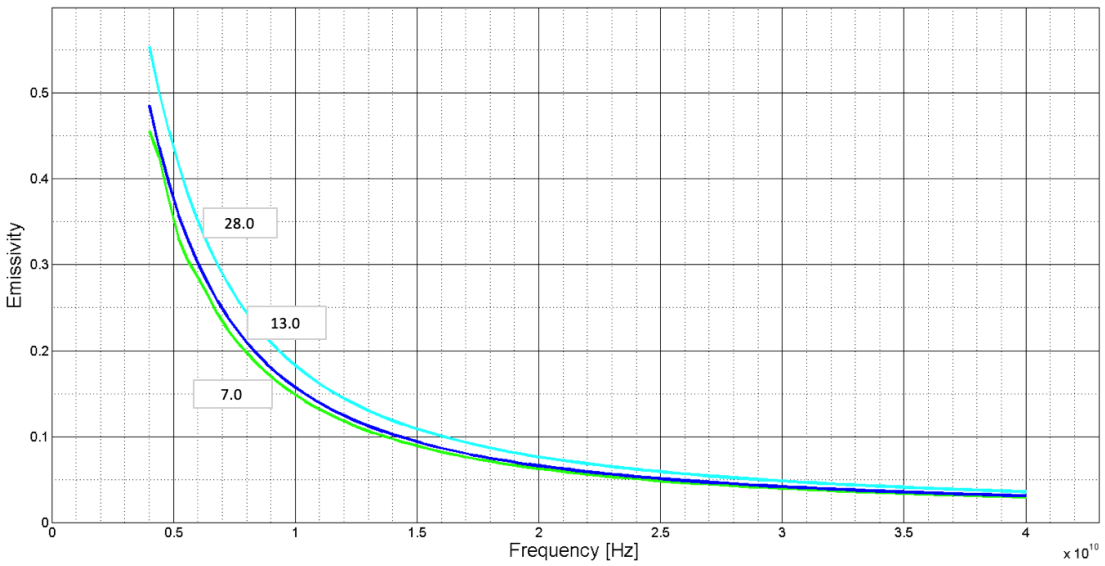

Figure 4.34. Emissivity versus frequency graph of branches and trunks with three values of ϵ_r'' for vertical polarization.

4.2.4. Emissivity versus Angle of Incidence - Vertical Polarization

Incident angle is considered as a second parameter in emissivity simulation of branch model. With different dimensions, frequencies and dielectric constants three graph was formed. The obvious effect of angle of incidence is an increase in emissivity. The geometry and therefore the effect on emissivity is different than leaf model.

Vertical polarization has a remarkable effect on leaf model simulations, however for cylinder vertical polarization results are almost the same with horizontal polarization case.

Table 4.8. Plotting parameters of emissivity versus angle of incidence graph of branch and trunk for vertical polarization.

Parameters	Graph.1	Graph.2	Graph.3	Graph.4
Radius of Leaf (a) (m)	a_v	0.02	0.02	0.02
Cylinder Length $(2l)$ (m)	l_v	1.00	1.00	1.00
Frequency (GHz)	10	f_v	10	10
Real Part (ϵ_r')	18.7	18.7	ϵ_v'	18.7
Imaginary Part (ϵ_r'')	7.0	7.0	7.0	ϵ_v''
# of Scatterers $(n\Delta z)$	32	32	64	64

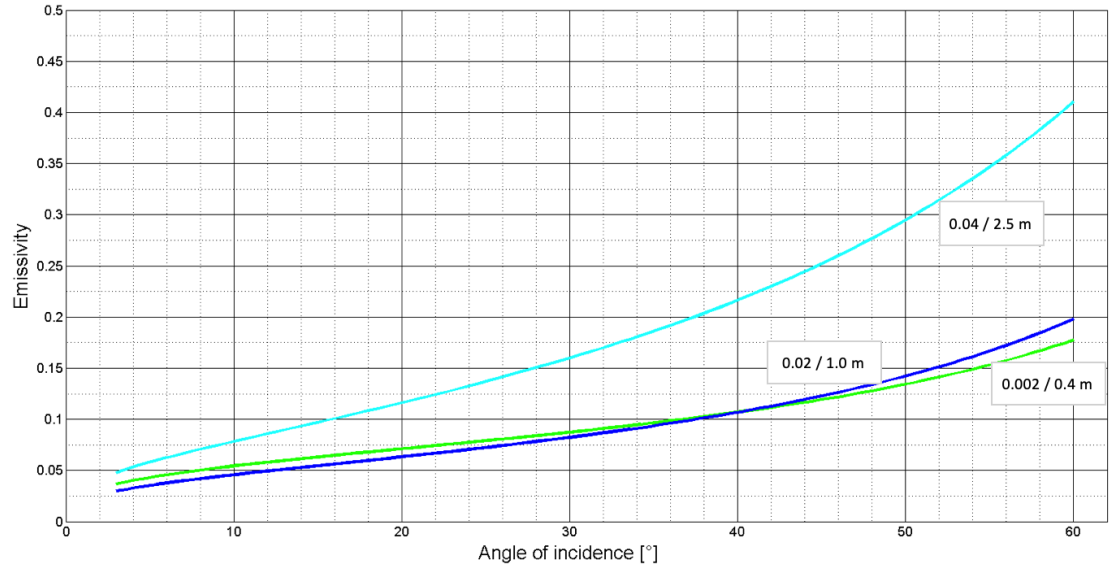

Figure 4.35. Emissivity versus angle of incidence graph of branches and trunks with three values of cylinder length and radius for vertical polarization.

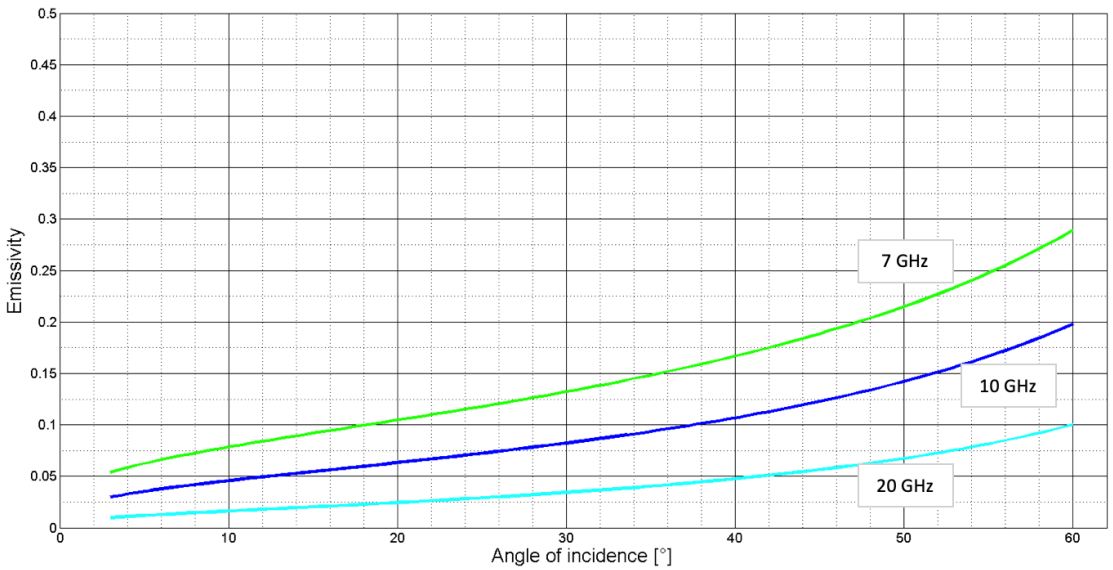

Figure 4.36. Emissivity versus angle of incidence graph of branches and trunks with three values of frequency for vertical polarization.

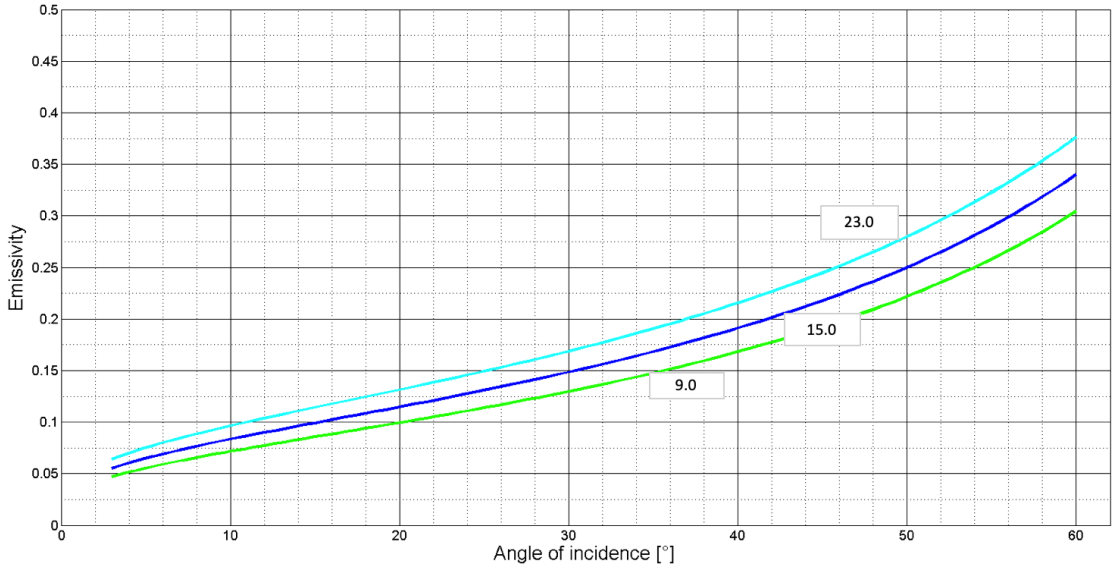

Figure 4.37. Emissivity versus angle of incidence graph of branches and trunks with three values of ϵ_r' for vertical polarization.

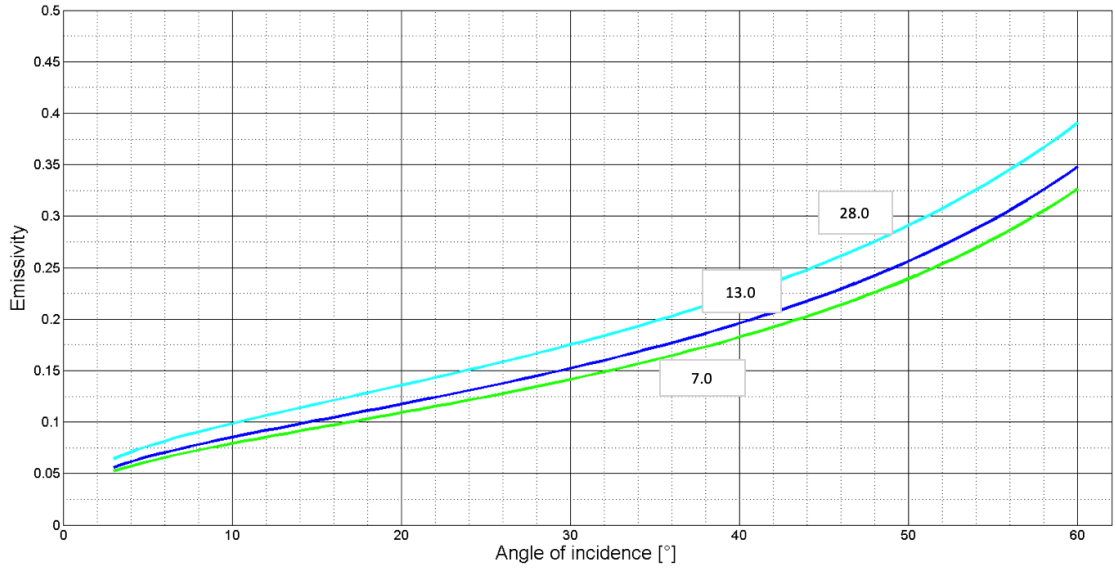

Figure 4.38. Emissivity versus angle of incidence graph of branches and trunks with three values of ϵ_r'' for vertical polarization.

4.3. Further Simulations for Human Model

In previous chapters, modeling and simulations for vegetation components are mentioned. Materials in the world are available as dielectric and magnetic materials. Many of these materials are present as dielectric materials. By the help of this simulation study, many dielectric materials can be modeled as disks and cylinders. For instance, a human body can be modeled as a cylinder of different dimensions. With this parametric study and developed MATLAB code, it is sufficient for modeling of objects with known of the dielectric constant and dimensions. In this section, as a study different from the thesis topic, modeling of human as a cylinder and simulations according to this model will be made and interpretation of the results will be realized.

Human body can be modeled as a cylinder, as it is given in Figure 4.39.

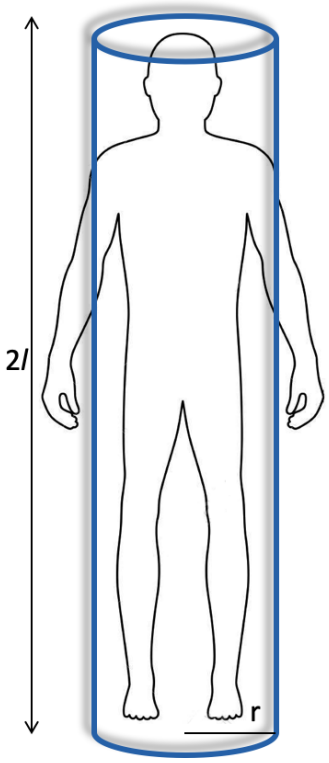

Figure 4.39. Human body modeled as a cylinder.

According to the data obtained in the literature, dielectric constant of the human body varies according to the body structure. In [59], there is two different values of dielectric constants measured for two different people. However, in this study it is assumed as the same for three example human model. Dielectric constant are calculated from the paper, [59], for the simulations below. Also, dielectric constant is assumed as a stable with changing frequency. The parameters of the modeled bodies are shown in Table 4.9.

Table 4.9. Human body model parameters.

	Length	Diameter	Dielectric Constant
1. Person	80 cm	10 cm	32 - i15.1
2. Person	160 cm	30 cm	32 - i15.1
3. Person	190 cm	50 cm	32 - i15.1

Using these parameters, simulations of the emissivity versus frequency of two modeled people with changing polarization is shown in Figure 4.40, Figure 4.41 and Figure 4.42. Angle of incidence is taken as 45^o, when these parameters are simulated, because of that our approximation about transmittance is proportional to cosines of the angle of incidence. Since, the approximation is not compatible for simulation in 90^o of angle of incidences.

Considering the results in these three figures, it appears that the emissivity decreases with increasing frequency. Vertical emissivity is higher than the horizontal polarization. In Figure 4.40, there is emissivity versus frequency simulation of horizontal and vertical polarization of a baby dimensions. Besides, in Figure 4.41, there is a woman and in Figure 4.42 there is a man, and his dimensions are considered in simulation. When these three figures are examined, it is seen that emissivity values are different but the curves are similar. Dimensions are different, so that the difference between emissivities of three model is related to the volume of the subject body. When these two figures examined, woman's emissivity is higher than the baby's. It is caused

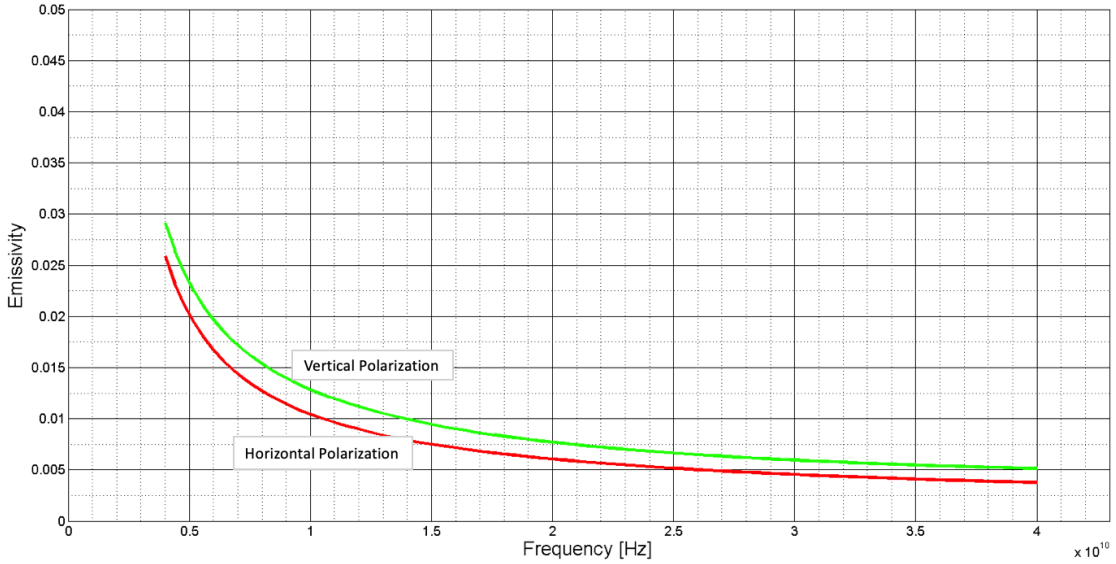

Figure 4.40. Emissivity versus frequency with horizontal and vertical polarizations for first person model.

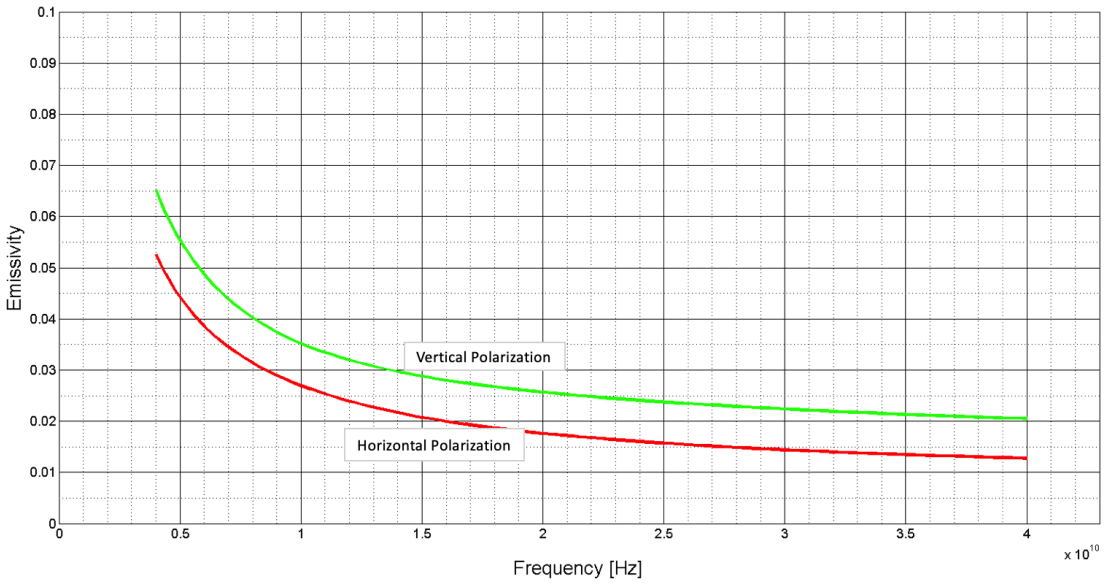

Figure 4.41. Emissivity versus frequency with horizontal and vertical polarizations for second person model.

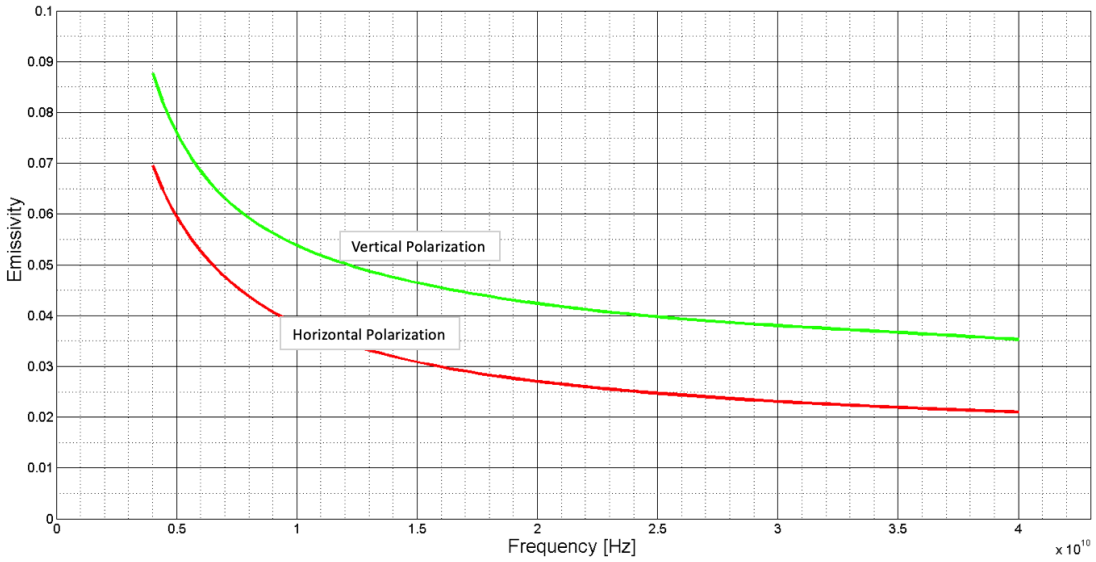

Figure 4.42. Emissivity versus frequency with horizontal and vertical polarizations for third person model.

from that in the ILC approximation formula to calculate electric field inside the cylinder. There is direct correlation between the volume of the object and the absorption cross sections. Thus the emissivity increased with the increased volume. The absorption cross sections are increased and also emissivity increased with increasing volume in the third model for man.

In these simulations, the human was modeled as a cylinder and its dielectric constant was taken constant for the entire human body. This approach is somewhat inadequate. In literature [60], there is a detailed measurement of the emissivity for the human arm and its different parts. They measure outer wrist, inner wrist, palm of hand, back of hand, dorsal surface and volar side of the arm separately in 80-100 GHz band.

Modeling of a single human as a single cylinder with single dielectric constant and calculated emissivity values may not provide us with much detailed information about the human being. In order to obtain detailed information about human, it

is necessary to model each part of human in various ways and make simulations on various dielectric constants. However, using the studies in this thesis, information on the number of people and the general statistics of that group can be provided. For example, when the other techniques are unable to determine the number and detailed information about the immigrants those are trying to enter in a country illegally, the method of this thesis study can be helpful for determining the number of children, women and men in this group. As a result for human model, this thesis study may not provide detailed information about human modeling alone, but it may provide some clues in modeling human as a group. More detailed studies are the subject of a further thesis.

5. CONCLUSION AND FUTURE WORK

5.1. Conclusions

In this thesis study, vegetation was modeled and modeled geometry was used to simulate emissivity of vegetation. As a passive remote sensing method, emissivity and absorption cross section were obtained from electric field definition inside the approximate model. In the beginning, emissivity equations were developed using reflection and transmission theory of electric field. The absorption cross section parameter in the emissivity equation was evaluated, so that the field inside the subject model was the challenging part.

Electric field inside a well defined shaped model can be extracted with some proper approximations. Approximations or assumptions were done in consistent with the frequency range and model geometry. In the first part, a leaf of the vegetation is modeled as thin and thick dielectric disks. Diameter of the disk and studied frequency range required physical optics approximation in calculation of internal electric field. Branches and trunks of vegetation was modeled as cylinders and for the calculation of cylinder absorption cross section, and therefore the field inside cylinder, infinite length cylinder approximation was utilized.

Model accuracy should be demonstrated, therefore created absorption cross section equations were simulated and calculated to make comparison with the results found from literature. Two studies were considered as basis for the comparison.At first, absorption cross section graph in [5] and simulated graph was compared. Results were consistent with that study. Secondly, absorption cross section was calculated for three frequency values with the same parameters in NASA report on high frequency scattering of dielectric disks [9]. Tables were created and error percentage was calculated for 1 GHz, 4 GHz and 7 GHz. Maximum error occurred at low frequency, the reason for that the restriction of approximation about the wavelength and radius of the disk.

In the simulation part of the study, emissivity of modeled compositions of vegetation was simulated. In each simulation, emissivity graph is found with a variable. In the first part, frequency of the incident field was the main variable and simulated for three different values of three variables of disk as the leaf model for horizontal and vertical polarizations. Similarly, angle of incidence were simulated as main variables in x axes of the graph.

In the leaf model, frequency was increased from 4 GHz to 40 GHz. Increase in frequency causes decrease in emissivity, except for one of the parameters. In the smallest value of real part of relative permittivity emissivity curve increases with decreasing slope and then stays constant for higher frequencies. Angle of incidence is the other parameter. Wide incidence angle has smaller value of emissivity. In horizontal polarization, emissivity value is greater at low frequencies. In vertical polarization, higher frequencies result in greater emissivity value, therefore depending on studied frequency range, horizontal and vertical polarizations could be applied in model. Effective results for emissivity could be obtained by investigating polarization. From the simulations, polarization has different effect on disk shaped model.

In the cylinder model constituted for branches and trunks, simulation parameters are similar. Length, radius, angle of incidence and relative permittivity are all second variables for curves. Vertical and horizontal polarization situations were considered separately. Emissivity curves for both polarizations are decreasing with increase in frequency. Angle of incidence is different than leaf model simulations. Wider incidence angle causes emissivity to increase.

Imaginary part of the dielectric constant constitutes energy loss in the material, therefore larger value of imaginary component causes increase in absorption therefore increase in emissivity. Real component describes the polarizability of material, large value of real part of dielectric constant results in different emissivity values for leaf, branches and trunk models.

As a further study, a human body was modeled as a cylinder and MATLAB simulations for this model was applied. Infinite length cylinder approximation was utilized for human body emissivity simulations. Emissivity versus frequency simulation for a baby, a woman and a man is examined. As a result, it is understood that modeling human as a single individual does not provide enough data for further studies. However, it will provide useful data for modeling a group of people in specific area. Because, as can be seen from the simulation results, the human size and average dielectric constant value has directly effect on the emissivity. As shown in the simulation results, the average dielectric constant of baby, woman and man were taken the same and only the sizes were different. The baby's emissivity value is lower than woman's. Also, man's emissivity value is higher than the others, because of the increased body volume. These results provide only general information for an individual person. In addition, these results will be useful in modeling a group of people.

In conclusion, this study provides a comprehensive work for vegetation emissivity. Emissivity, absorption cross section and electric field inside dielectric material was studied. For two main components of vegetation, absorption cross section and emissivity equations were presented. MATLAB was used to simulate these equations with vegetation parameters. Simulations were evaluated and commented.

5.2. Future Work

Emissivity and vegetation modeling study was brought to a stage with this thesis work that provides a collected method for object modeling in passive remote sensing. In passive remote sensing, emissivity and absorption cross section parameters are important indicators about properties of the subject material.

Materials in the world are available as dielectric and magnetic materials. Many of these materials are present as dielectric materials. By the help of this simulation study, many dielectric materials can be modeled as disks and cylinders. With this parametric study, it is sufficient for modeling to know the dielectric constant and dimensions. Furthermore, absorption and scattering characteristics of an object can

also be examined with the help of this comprehensive study.

In addition, with using this study, a further study can be done about the soil and underground resources where plants grow. For example, at first, the emissivity values of a tree grown under control can be taken as basis. Subsequently, assumptions can be made about the minerals found in soil and underground mines by changing the emission measurements of the areas of the same tree species. The variable dielectric value of this tree can be calculated from the variable emissivity values. Thus, the mineral content in the tree can be determined by changing the dielectric properties. It is the signature of the mineral content of the soil where is that tree grown. In the next study, when minerals are discovered in the soil, fruit and vegetables that can grow most efficiently in this region can be identified. This study can help governments determine agricultural policy. In addition, if an underground mine is detected in the calculations, a resource for the public can be created.

REFERENCES

1. Halpern, J. B., "Libretexts: a flexible online open system for disseminating educational materials relevant to geophysics at all levels", *AGU Fall Meeting Abstracts*, 2017.

2. Duband, L., "Space cryocooler developments", *Physics Procedia*, Vol. 67, pp. 1–10, 2015.

3. National Academies of Sciences, E., Medicine *et al.*, *A Strategy for Active Remote Sensing Amid Increased Demand for Radio Spectrum*, National Academies Press, 2015.

4. Tindall, J. A., *Deconvolution of plant type (s) for homeland security enforcement using remote sensing on a uav collection platform*, Tech. rep., GEOLOGICAL SURVEY DENVER CO, 2006.

5. Seker, S. S., *Resonant Backscattering From Sparsely Distributed Lossy Dielectric Scatterers.*, Ph.D. Thesis, The George Washington University, 1982.

6. Ulaby, F. T., R. K. Moore and A. K. Fung, *Microwave Remote Sensing-Active and Passive-Volume I-Microwave Remote Sensing Fundamentals and Radiometry (v. 1)*, 1981.

7. Campbell, J. B. and R. H. Wynne, *Introduction to remote sensing*, Guilford Press, 2011.

8. Andersen, H.-E., S. E. Reutebuch and R. J. McGaughey, "Active remote sensing", *Computer applications in sustainable forest management*, pp. 43–66, Springer, 2006.

9. LeVine, D., R. Meneghini, R. Lang and S. Seker, "High frequency scattering from

arbitrarily oriented dielectric disks", *NASA Technical Report*, 1982.

10. Joseph, G., *Fundamentals of remote sensing*, Universities press, 2005.

11. Liou, K.-N., *An introduction to atmospheric radiation*, Vol. 84, Elsevier, 2002.

12. Elachi, C. and J. J. Van Zyl, *Introduction to the physics and techniques of remote sensing*, Vol. 28, John Wiley & Sons, 2006.

13. Horvath, H., "Atmospheric light absorption: A review", *Atmospheric Environment. Part A. General Topics*, Vol. 27, No. 3, pp. 293–317, 1993.

14. Turco, R. P., *Earth under siege: From air pollution to global change*, Oxford University Press, 1997.

15. Clark, R. N. *et al.*, "Spectroscopy of rocks and minerals, and principles of spectroscopy", *Manual of remote sensing*, Vol. 3, No. 3-58, pp. 2–2, 1999.

16. Tsang, L., J. Kong and R. Shin, *Theory of Microwave Remote Sensing*, Wiley Series in Remote Sensing and Image Processing, Wiley, 1985.

17. Sharkov, E. A., *Passive microwave remote sensing of the Earth: physical foundations*, Springer Science & Business Media, 2003.

18. Pettorelli, N., H. Schulte to Bühne, A. Tulloch, G. Dubois, C. Macinnis-Ng, A. M. Queirós, D. A. Keith, M. Wegmann, F. Schrodt, M. Stellmes *et al.*, "Satellite remote sensing of ecosystem functions: opportunities, challenges and way forward", *Remote Sensing in Ecology and Conservation*, Vol. 4, No. 2, pp. 71–93, 2018.

19. Woodhouse, I. H., *Introduction to microwave remote sensing*, CRC press, 2017.

20. Ulaby, F. T., R. K. Moore and A. K. Fung, *Microwave remote sensing: active and passive. Vol. 2, Radar remote sensing and surface scattering and emission theory*, Addison-Wesley Reading, MA, 1982.

21. Kumar, D. N. and T. Reshmidevi, "Remote sensing applications in water resources", *Journal of the Indian Institute of Science*, Vol. 93, No. 2, pp. 163–188, 2013.

22. Wolfe, D., A. Larraza and A. Garcia, "A horizontal vane radiometer: Experiment, theory, and simulation", *Physics of Fluids*, Vol. 28, No. 3, p. 037103, 2016.

23. Cavalieri, D. J. and T. Markus, "EOS Aqua AMSR-E Arctic Sea Ice Validation Program: Arctic2003 Aircraft Campaign Flight Report", *NASA Report*, 2003.

24. Skou, N. and D. Vine, *Microwave Radiometer Systems: Design and Analysis*, Artech House remote sensing library, Artech House, 2006.

25. Sabins, F. F., "Remote sensing for mineral exploration", *Ore Geology Reviews*, Vol. 14, No. 3-4, pp. 157–183, 1999.

26. Seto, S., *Soil moisture estimation by microwave remote sensing on global scale*, Ph.D. Thesis, Ph. D. thesis, University of Tokyo, 2003.

27. Robinson, I. S., "The methods of satellite oceanography", *Discovering the Ocean from Space*, pp. 7–67, Springer, 2010.

28. Seker, S., M. E. Aydemir and G. Apaydin, "A Simulation Study for Computing the Emissivity of Clouds", *Acta Polytechnica*, Vol. 43, No. 3, 2003.

29. Moghaddam, M., A. Tabatabaeenejad, R. Chen, R. Akbar and A. Silva, "Role of computational EM in radar remote sensing of water resources", *Computational Electromagnetics (ICCEM), 2017 IEEE International Conference on*, pp. 331–332, IEEE, 2017.

30. Simonovic, S. P. *et al.*, *Role of remote sensing in disaster management*, Department of Civil and Environmental Engineering, The University of Western Ontario, 2002.

31. Pettorelli, N., K. Safi and W. Turner, "Satellite remote sensing, biodiversity re-

search and conservation of the future", *Philosophical Transactions*.

32. Ballew, L. R., *A microwave radiometer system for use in biomedical applications.*, Ph.D. Thesis, 2006.

33. Xiao, Y. and Q. Zhan, "A review of remote sensing applications in urban planning and management in China", *Urban Remote Sensing Event, 2009 Joint*, pp. 1–5, IEEE, 2009.

34. Chen, L., C. Wang and Q. Cui, "A multi-order radiative transfer model for microwave radiometry of vegetation canopies", *Antennas, Propagation and EM Theory (ISAPE), 2016 11th International Symposium on*, pp. 921–924, IEEE, 2016.

35. Martinez-Vazquez, A., A. Camps, N. Duffo, M. Vall-Ilossera and J. López-Sánchez, "Full polarimetric emissivity of vegetation-covered soils: Vegetation structure effects", *Geoscience and Remote Sensing Symposium, 2002. IGARSS'02. 2002 IEEE International*, Vol. 6, pp. 3542–3544, IEEE, 2002.

36. Xie, Y., J. Shi, Y. Lei and Y. Li, "Modeling Microwave Emission from Short Vegetation-Covered Surfaces", *Remote Sensing*, Vol. 7, No. 10, pp. 14099–14118, 2015.

37. Jackson, T. J. and P. E. O'Neill, "Microwave emission and crop residues", *Remote sensing of environment*, Vol. 36, No. 2, pp. 129–136, 1991.

38. Saatchi, S. S., D. M. Le Vine and R. H. Lang, "Microwave backscattering and emission model for grass canopies", *IEEE Transactions on Geoscience and Remote Sensing*, Vol. 32, No. 1, pp. 177–186, 1994.

39. Calla, O., A. R. Rai, P. Mathur, D. Mathur and D. Bohra, "Estimation of emissivity and scattering coefficient of the constituents of vegetation at microwave frequencies", *78.20 Ci; 84.40 Xb*, 2005.

40. Helhel, S., B. Colak and S. Ozen, "Measurement of dielectric constant of thin leaves by moisture content at 4mm band", *Progress In Electromagnetics Research*, Vol. 7, pp. 183–191, 2009.

41. Matzler, C., "Microwave (1-100 GHz) dielectric model of leaves", *IEEE Transactions on Geoscience and Remote Sensing*, Vol. 32, No. 4, pp. 947–949, 1994.

42. López, A., F. Molina-Aiz, D. Valera and A. Peña, "Determining the emissivity of the leaves of nine horticultural crops by means of infrared thermography", *Scientia Horticulturae*, Vol. 137, pp. 49–58, 2012.

43. Min, Q., B. Lin and R. Li, "Remote sensing vegetation hydrological states using passive microwave measurements", *IEEE Journal of Selected Topics in Applied Earth Observations and Remote Sensing*, Vol. 3, No. 1, pp. 124–131, 2010.

44. Gausman, H. and W. Allen, "Optical parameters of leaves of 30 plant species", *Plant Physiology*, Vol. 52, No. 1, pp. 57–62, 1973.

45. Neinavaz, E., *Sensing vegetation canopies in the thermal domain*, University of Twente Faculty of Geo-Information and Earth Observation (ITC), 2017.

46. Karam, M. A., "A physical model for microwave radiometry of vegetation", *IEEE Transactions on Geoscience and Remote Sensing*, Vol. 35, No. 4, pp. 1045–1058, 1997.

47. Peake, W., "Interaction of electromagnetic waves with some natural surfaces", *IRE Transactions on Antennas and Propagation*, Vol. 7, No. 5, pp. 324–329, 1959.

48. Adibekyan, A., *High-accuracy Spectral Emissivity Measurement for Industrial and Remote Sensing Applications*, Ph.D. Thesis, Universität Wuppertal, Fakultät für Mathematik und Naturwissenschaften, 2018.

49. Ulaby, F. T., E. Michielssen and U. Ravaioli, *Fundamentals of applied electromag-*

netics 6e, 2010.

50. Ulaby, F. T., R. K. Moore and A. K. Fung, *Microwave remote sensing active and passive-volume III: from theory to applications*, Artech House, Inc, 1986.

51. Seker, S. and O. Cerezci, "A simulation study of the cloud propagation model", *Journal of Physics D: Applied Physics*, Vol. 32, No. 5, p. 552, 1999.

52. Ulaby, F. T., U. Ravaioli and E. Michielssen, *Fundamentals of applied electromagnetics*, Prentice Hall, 2014.

53. LeVine, D., R. Meneghini, R. Lang and S. Seker, "Scattering from arbitrarily oriented dielectric disks in the physical optics regime", *JOSA*, Vol. 73, No. 10, pp. 1255–1262, 1983.

54. Ferrazzoli, P. and L. Guerriero, "Emissivity of vegetation: theory and computational aspects", *Journal of Electromagnetic Waves and Applications*, Vol. 10, No. 5, pp. 609–628, 1996.

55. Wolf, E. and M. Born, *Principles of optics*, Vol. 5, Pergamon press, 1965.

56. Wait, J. R., "Electromagnetic radiation from cylindrical structures", *NASA STI/Recon Technical Report A*, Vol. 89, 1988.

57. Mashhadi, M., A. Abdolali and N. Komjani, "Electromagnetic wave scattering from cylindrical structure with mixed-impedance boundary conditions", *Progress In Electromagnetics Research*, Vol. 29, pp. 207–222, 2013.

58. Release, M., "The mathworks", *Inc., Natick, Massachusetts, United States*, Vol. 488, 2013.

59. Wu, T., T. S. Rappaport and C. M. Collins, "The human body and millimeter-wave wireless communication systems: Interactions and implications", *2015 IEEE International Conference on Communications (ICC)*, pp. 2423–2429, IEEE, 2015.

60. Owda, A. Y., N. Salmon and N. D. Rezgui, "Electromagnetic signatures of human skin in the millimeter wave band 80-100 GHz", *Progress In Electromagnetics Research*, Vol. 80, pp. 79–99, 2018.